Published for SISSA by Springer

Received: December 30, 2022
Revised: October 11, 2023
Accepted: October 27, 2023
Published: November 20, 2023

Electroweak corrections to $g + g \to H_{l,h}$ and $H_{l,h} \to \gamma + \gamma$ in the Higgs-singlet extension of the Standard model

Christian Sturm,[a] **Benjamin Summ**[a] **and Sandro Uccirati**[b]

[a] *Lehrstuhl für Theoretische Physik II, Institut für Theoretische Physik und Astrophysik, Universität Würzburg, Campus Hubland Nord, Emil-Hilb-Weg 22, D-97074 Würzburg, Germany*

[b] *Dipartimento di Fisica, Universit'a di Torino, and INFN, Sezione di Torino, Via P. Giuria 1, I-10125 Torino, Italy*

E-mail: Christian.Sturm@physik.uni-wuerzburg.de, Benjamin.Summ@physik.uni-wuerzburg.de, uccirati@to.infn.it

Abstract: We calculate the next-to-leading order electroweak corrections for Higgs-boson production in gluon fusion and the Higgs-boson decay into two photons or gluons in the real Higgs-singlet extension of the Standard model (HSESM). For the light Higgs-boson of the HSESM the electroweak corrections for these processes are of the same order of magnitude as in the Standard model. For the heavy Higgs-boson of the HSESM the electroweak corrections can become large depending on the considered scenario.

Keywords: Electroweak Precision Physics, Higher Order Electroweak Calculations, Multi-Higgs Models, Specific BSM Phenomenology

ArXiv ePrint: 2212.11835

https://doi.org/10.1007/JHEP11(2023)113

JHEP11(2023)113

Contents

1 Introduction

The discovery of a Higgs boson at the Large Hadron Collider (LHC) [1, 2] was a tremendous success and the beginning of detailed studies of its properties. One important question is, whether the discovered Higgs boson is just the Standard model (SM) Higgs boson or whether it is part of a more general Higgs sector. One of the simplest extensions of the SM Higgs sector is the one where one adds an additional electroweak scalar singlet field S to the SM field content [3–9].

In general one can distinguish two types of Higgs-Singlet Extensions of the SM (HSESM); the real singlet extension of the SM and the complex singlet extension of the SM. In the case of the real HSESM one has one additional physical Higgs boson with respect to the Standard Model. Since a second physical Higgs boson lighter than the discovered one is strongly constrained [10],[1] in this work we consider it as heavy (and call it H_h) compared to the light observed Higgs boson H_l with mass $M_{H_l} \equiv M_h = 125.25\,\text{GeV}$ [12]. In the real HSESM one has only three new additional free parameters compared to the SM, which can be expressed in terms of the new heavy Higgs-boson mass M_{H_h}, the ratio of two vacuum expectation values, conventionally denoted by $\tan\beta$, and a mixing angle α. The complex HSESM can have in addition other free parameters [13]. For certain configurations of these parameters the HSESM can provide candidates for dark matter. In the following we will consider a real scalar Higgs singlet S which has a vacuum expectation value (vev) as well

[1] We acknowledge that recent studies show that in some regions of the parameter space the constraints for a high M_{H_h} can also be strong, cf. e.g. [11].

JHEP11(2023)113

as a discrete Z_2 symmetry, $S \to -S$, so that terms which are odd in S do not appear in the potential. Searches for a new scalar resonance are being scrutinized by the ATLAS and CMS collaborations [14–20] by deriving bounds and constraints on the new parameters of the HSESM [21].

Next-to-leading order (NLO) electroweak (EW) corrections to light and heavy Higgs-boson production in Higgs strahlung and to Higgs-boson production in vector-boson fusion as well as the NLO results on the four-fermion (f) decays $H_{l,h} \to WW/ZZ \to 4f$ have been computed in refs. [22–24]. Interference effects at the one-loop level for the W^+W^-, $t\bar{t}$ and HH decay modes have been studied in refs. [25, 26]. NLO electroweak corrections to the heavy-to-light Higgs-boson decay have been determined in ref. [27]. The low energy behaviour of the HSESM has been studied in refs. [28–32] and references therein.

Theoretical and experimental constraints and their impact on the allowed parameter space as well as benchmark scenarios for searches for an additional Higgs singlet have been studied in refs. [33–37]. Several benchmark scenarios have been summarized in the report of the LHC Higgs Cross section Working Group (HXSWG) [38].

Within this work we focus on the loop-induced Higgs-boson production and decay processes. In the SM NLO electroweak corrections to Higgs-boson production in gluon fusion and the Higgs-boson decay into two photons are known since long [39–43]. The QCD corrections to both processes have been computed up to N^{3}LO [44–47] and turn out to be very large for gluon fusion increasing the cross section by about a factor of 2, while for $H \to \gamma\gamma$ they are comparable to the NLO electroweak ones. The mixed QCD-electroweak corrections for Higgs-boson production, known at three loops, are of the same order of the QCD ones [48]. In the HSESM theory predictions for cross sections of Higgs-boson production via gluon fusion at higher order in perturbative QCD can be obtained from the SM results, whereas higher order electroweak corrections in this model are still unknown for this process. In this paper we calculate the effect of the NLO electroweak corrections on the production of a light and a heavy Higgs boson through gluon (g) fusion, $g + g \to H_{l,h}$, in the real HSESM. Likewise we calculate the NLO electroweak correction of the Higgs-boson decay into two photons (γ) in the real HSESM for the light and heavy Higgs boson, $H_{l,h} \to \gamma + \gamma$, which are also still unknown. The few new parameters in the model under consideration will allow us then to provide even scans over a wide range of the new input parameters, rather than restricting ourselves to benchmark points only, which makes our results more generally applicable, if further parameter regions will be experimentally excluded. In addition we provide results for the benchmark points collected in refs. [23, 37, 38], which we will outline in more detail later in this work.

Electroweak corrections to loop-induced Higgs-boson production and decay processes can become large. This has been seen, for example, in the calculation of the electroweak corrections to Higgs-boson production through gluon fusion and the Higgs-boson decay into two photons in a SM with a sequential fourth generation of heavy fermions [49, 50]. Similarly the calculation of the two-loop, electroweak corrections to the production of a light and a heavy neutral, scalar Higgs-boson through the gluon fusion process in the Two-Higgs-Doublet Model(2HDM) [51–53] also showed that the corrections can be sizable. The knowledge of the electroweak corrections in the HSESM is thus important.

JHEP11(2023)113

The outline of this paper is as follows. In section 2 we define the HSESM and its new parameters. Section 3 contains the details of our calculations and checks which we have performed. In section 4 we present our results and discuss them. Finally we close with our summary and conclusions in section 5.

2 The Higgs-singlet extension of the Standard model

The scalar potential of the Higgs-Singlet Extensions of the SM (HSESM), which satisfies a Z_2 symmetry, $S \to -S$, is given by

$$V_{\text{HSESM}} = m_1^2 \Phi^\dagger \Phi + m_2^2 S^2 + \frac{\lambda_1}{2}\left(\Phi^\dagger \Phi\right)^2 + \frac{\lambda_2}{2} S^4 + \lambda_3 \Phi^\dagger \Phi S^2, \tag{2.1}$$

where we have adopted the conventions of ref. [22] with the scalar doublet field Φ and the scalar singlet field S. The parameters m_1^2, m_2^2 and λ_i $(i = 1, 2, 3)$ of the potential are all real. For

$$\lambda_1 > 0, \quad \lambda_2 > 0 \quad \text{and} \quad \lambda_3^2 < \lambda_1 \lambda_2 \tag{2.2}$$

the potential has a global minimum with non-vanishing vacuum expectation values (vevs) of the scalar fields. The last inequality follows from the requirement that the Hessian matrix is positive definite at the extremum. The Hessian matrix is up to a global factor the mass (squared) matrix M_{ij}^2 from eq. (2.5) below. It is real symmetric and thus orthogonal diagonalizable with real eigenvalues.

The Higgs doublet Φ and the Higgs singlet S are parameterized as

$$\Phi = \begin{pmatrix} \phi^+ \\ \frac{1}{\sqrt{2}}(v + \rho_1 + \mathrm{i}\eta) \end{pmatrix}, \qquad S = \frac{v_S + \rho_2}{\sqrt{2}}, \tag{2.3}$$

respectively, where η and $\phi^\pm$ are the would-be Goldstone-boson fields. Here, v and v_S are vacuum expectation values whose ratio is defined as $t_\beta \equiv \tan\beta = v_S/v$. The limit $t_\beta \to 0$ corresponds to the limit of a vanishing vev $v_S \to 0$. After spontaneous symmetry breaking the real fields ρ_1 and ρ_2 mix to produce the mass eigenstates H_{h} and H_{l} through a orthogonal matrix

$$\begin{pmatrix} \rho_1 \\ \rho_2 \end{pmatrix} = \begin{pmatrix} \cos\alpha & -\sin\alpha \\ \sin\alpha & \cos\alpha \end{pmatrix} \begin{pmatrix} H_{\text{l}} \\ H_{\text{h}} \end{pmatrix}. \tag{2.4}$$

This rotation to the mass eigenstates diagonalizes the mass (squared) matrix

$$M_{ij}^2 = \left.\frac{\partial^2 V_{\text{HSESM}}}{\partial\rho_i \partial\rho_j}\right|_{\rho_{i,j}=0,\eta=0,\phi^\pm=0}, \qquad (i, j = 1, 2), \tag{2.5}$$

which has eigenvalues $M_{H_{\text{l}}}^2$ and $M_{H_{\text{h}}}^2$ that satisfy $M_{H_{\text{l}}} < M_{H_{\text{h}}}$. The angle α is restricted to the interval $(-\pi/2, \pi/2]$. The real scalar fields satisfy the minimum conditions for the scalar potential

$$\langle \rho_i \rangle = 0, \quad (i = 1, 2). \tag{2.6}$$

JHEP11(2023)113

Using these conditions and the rotation into the basis of mass eigenstates one can express the potential parameters through the physical input parameters, i.e. the masses of the light and heavy Higgs boson, M_{H_l} and M_{H_h} as well as the mixing angle α, the ratio of the vevs $\tan\beta$ and the vev v. The quartic couplings take the form

$$\lambda_1 = \frac{M_{H_\mathrm{l}}^2}{v^2}\cos^2\alpha + \frac{M_{H_\mathrm{h}}^2}{v^2}\sin^2\alpha, \tag{2.7}$$

$$\lambda_2 = \frac{M_{H_\mathrm{l}}^2}{v^2\tan^2\beta}\sin^2\alpha + \frac{M_{H_\mathrm{h}}^2}{v^2\tan^2\beta}\cos^2\alpha, \tag{2.8}$$

$$\lambda_3 = \frac{M_{H_\mathrm{l}}^2 - M_{H_\mathrm{h}}^2}{2v^2\tan\beta}\sin(2\alpha). \tag{2.9}$$

Instead of the ratio of the vevs $\tan\beta$ one can also use λ_3 as an input parameter by expressing $\tan\beta$ in terms of λ_3 with the help of eq. (2.9). As per usual the vev v is fixed through its relation to the W-boson mass M_W and the weak isospin gauge coupling g, which is the same in the HSESM as in the SM

$$M_W = \frac{1}{2}gv. \tag{2.10}$$

As can be seen from eq. (2.8) the coupling λ_2 is quadratically enhanced(suppressed) for small(large) values of $\tan\beta$. The coupling λ_3 is the only coupling of the Higgs sector that depends on the sign of the mixing angle α. If the mixing angle α is negative(positive), the coupling λ_3 of eq. (2.9) is always positive(negative), since $M_{H_\mathrm{l}} < M_{H_\mathrm{h}}$ and $\tan\beta > 0$. The inequalities in (2.2) are equivalent to requiring that the quadratic physical Higgs-boson masses are positive. Inserting eqs. (2.7)–(2.8) into the expressions for $m_{1,2}$ derived from the extremal condition of the potential one finds

$$m_1^2 = -\frac{M_{H_\mathrm{l}}^2\cos^2\alpha + M_{H_\mathrm{h}}^2\sin^2\alpha}{2} + \frac{M_{H_\mathrm{h}}^2 - M_{H_\mathrm{l}}^2}{4}\sin(2\alpha)\tan\beta, \tag{2.11}$$

$$m_2^2 = -\frac{M_{H_\mathrm{h}}^2\cos^2\alpha + M_{H_\mathrm{l}}^2\sin^2\alpha}{2} + \frac{M_{H_\mathrm{h}}^2 - M_{H_\mathrm{l}}^2}{4}\frac{\sin(2\alpha)}{\tan\beta}. \tag{2.12}$$

We have assumed to have two non-vanishing vevs, so that one can expect that at least one of the two parameter m_1^2 and m_2^2 has to be negative,[2] however the other can also be positive.

Note that the doublet Φ couples to gauge bosons and fermions in exactly the same way as in the SM and the only effect of the Higgs singlet is that there is Higgs mixing. Therefore the tree-level couplings of H_l and H_h to gauge bosons and fermions are the same as those of the SM Higgs boson, but scaled by the respective trigonometric function of the mixing angle α. We also note that t_β only appears in purely scalar tree-level vertices, which are polynomials of degree at most two in $1/t_\beta$.

[2] If we assumed that m_1^2 and m_2^2 are both positive and use λ_3 from eq. (2.9), this would lead to

$$-\frac{(M_{H_\mathrm{h}}^2 - M_{H_\mathrm{l}}^2)^2\sin^2(2\alpha)}{4v^2(M_{H_\mathrm{l}}^2\cos^2\alpha + M_{H_\mathrm{h}}^2\sin^2\alpha)} < \lambda_3 < -\frac{M_{H_\mathrm{h}}^2\cos^2\alpha + M_{H_\mathrm{l}}^2\sin^2\alpha}{v^2}.$$

Multiplying this inequality by the positive factor $M_{H_\mathrm{l}}^2\cos^2\alpha + M_{H_\mathrm{h}}^2\sin^2\alpha$ one can see that the upper bound of λ_3 is smaller than the lower bound, leading to a contradiction.

JHEP11(2023)113

3 Calculation

3.1 Generalities

The leading-order (LO) partial decay width Γ of a Higgs boson H of the HSESM decaying into two photons (γ) can be expressed by modifying the SM result [54, 55] and is given by

$$\Gamma^{\mathrm{LO}}_{\mathrm{HSESM}}(H \to \gamma + \gamma) = \frac{G_F M_H^3 \alpha_{\mathrm{em}}^2}{32\sqrt{2}\pi^3} c_H^2 |A^{\mathrm{LO}}_{\gamma\gamma}|^2, \tag{3.1}$$

where H stands here and in the following for either the light or the heavy Higgs boson, H_{l} or H_{h}; G_F is the Fermi-coupling constant and α_{em} the fine-structure constant. The coefficient c_H is given by

$$c_{H_{\mathrm{l}}} = \cos(\alpha), \qquad c_{H_{\mathrm{h}}} = -\sin(\alpha), \tag{3.2}$$

where the SM limit corresponds to $\sin\alpha \to 0$, $\cos\alpha \to 1$ and is at LO independent of $\tan\beta$. Considering NLO electroweak corrections in the renormalization schemes described in section 3.3, the new Higgs sector decouples for our processes when sending in addition $\tan\beta \to \infty$, since in the limit $\tan\beta \to \infty$ the vertices which mix different Higgs bosons vanish and $\tan\beta$ only appears in purely scalar tree-level vertices. The dimensionless amplitude $A^{\mathrm{LO}}_{\gamma\gamma}$ can be decomposed into a fermionic (fer) and bosonic (bos) contribution $A^{\mathrm{LO}}_{\gamma\gamma} = A_{\mathrm{fer}} + A_{\mathrm{bos}}$. The fermionic contribution can again be subdivided into a part which arises from leptons A_l and one which arises from quarks A_q, i.e. $A_{\mathrm{fer}} = \sum_l Q_l^2 A_l + N_c \sum_q Q_q^2 A_q$, where Q_l and Q_q are the electric charges of the fermions in units of the elementary charge and N_c is the number of colours. The sum runs over all charged leptons l and quarks q. We only consider the top quark as massive and all other fermions as massless, so that only the term containing A_{top} will contribute to the dimensionless fermionic amplitude A_{fer}. Under these assumptions the dimensionless fermionic and bosonic amplitudes read

$$A_{\mathrm{bos}}(\tau_W) = -1 - \frac{3}{2\tau_W}\left[1 + \left(2 - \frac{1}{\tau_W}\right) f(\tau_W)\right], \tag{3.3}$$

$$A_{\mathrm{top}}(\tau_t) = \frac{1}{\tau_t}\left[1 + \left(1 - \frac{1}{\tau_t}\right) f(\tau_t)\right], \tag{3.4}$$

with $\tau_p = M_H^2/(4M_p^2)$ ($p \in \{t, W\}$). The function $f(\tau)$ is given by

$$f(\tau_p) = \begin{cases} \arcsin^2\sqrt{\tau_p}, & \text{if } \tau_p \le 1, \\ -\frac{1}{4}\left[\ln\left(\frac{1+\sqrt{1-1/\tau_p}}{1-\sqrt{1-1/\tau_p}}\right) - \mathrm{i}\pi\right]^2, & \text{if } \tau_p > 1. \end{cases} \tag{3.5}$$

The real and imaginary parts of the purely bosonic and fermionic dimensionless amplitudes of eqs. (3.3) and (3.4) have opposite signs in the whole Higgs-boson mass range, see figure 1. For the numerical evaluation in figure 1 as well as in the following figures 2 and 3 we use the masses in the complex mass scheme, which will be discussed in section 3.3. The input parameters used for the numerical evaluations are from the PDG [12] for the particle masses

JHEP11(2023)113

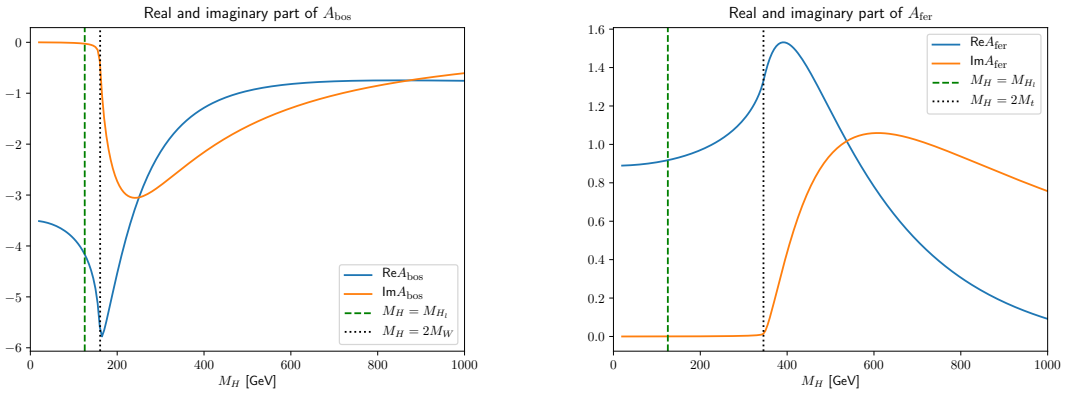

(a) (b)

Figure 1. Real (a) and imaginary (b) part of the bosonic and fermionic contribution to $A_{\gamma\gamma}^{\text{LO}}$, respectively. The vertical dashed line denotes the location of the SM Higgs-boson $M_H = M_{H_l} = 125.25\,\text{GeV}$. The vertical dotted lines indicate the location of the WW- and $t\bar{t}$-thresholds. The dimensionless amplitudes are evaluated with complex masses as described in section 3.2.

and their total decay widths and read:

$$\begin{aligned} M_t &= 172.76\ \text{GeV}, & M_Z &= 91.1876\ \text{GeV}, & M_W &= 80.379\ \text{GeV}, \\ \Gamma_t &= 1.42\ \text{GeV}, & \Gamma_Z &= 2.4952\ \text{GeV}, & \Gamma_W &= 2.085\ \text{GeV}, \\ M_{H_l} &= 125.25\ \text{GeV}, & \Gamma_{H_l} &= 0.0032\ \text{GeV}, & G_F &= 1.1663787 \cdot 10^{-5}\ \text{GeV}^{-2}, \\ \alpha_s(M_Z) &= 0.1179, & \alpha_{\text{em}} &= 1/137.035999084. \end{aligned} \tag{3.6}$$

From figure 1 we see that the imaginary parts are zero below the WW and $t\bar{t}$ threshold, respectively, up to tiny contributions from the finite widths in the complex mass scheme. In particular for Higgs-boson masses above about $M_H \approx 500\,\text{GeV}$ one can observe strong cancellations between the dimensionless bosonic and fermionic amplitude, so that the real and imaginary parts of the total dimensionless amplitude have modulus smaller than one, see figure 2(a). Therefore the modulus squared of the total dimensionless amplitude is very small in this mass range, see figure 2(b). Such cancellations, which lead to a small dimensionless LO amplitude, can cause the relative NLO corrections to be huge, although the absolute size of the NLO corrections is reasonable. We will observe exactly this situation in section 4.2. A similar observation was made in studying a sequential fourth generation of heavy fermions [50]. In addition to these cancellations there is a minimum of the modulus squared of the dimensionless amplitude around $M_H \sim 630 - 640\,\text{GeV}$, see inset of figure 2(b), which is even more enhanced[3] for the decay width of a heavy Higgs-boson, as can be seen in figure 3(a). The leading-order cross section for the production of a Higgs boson H of the

[3]The reason for the enhancement is the overall factor of M_H^3 in eq. (3.1) which causes the grow after the minimum.

JHEP11(2023)113

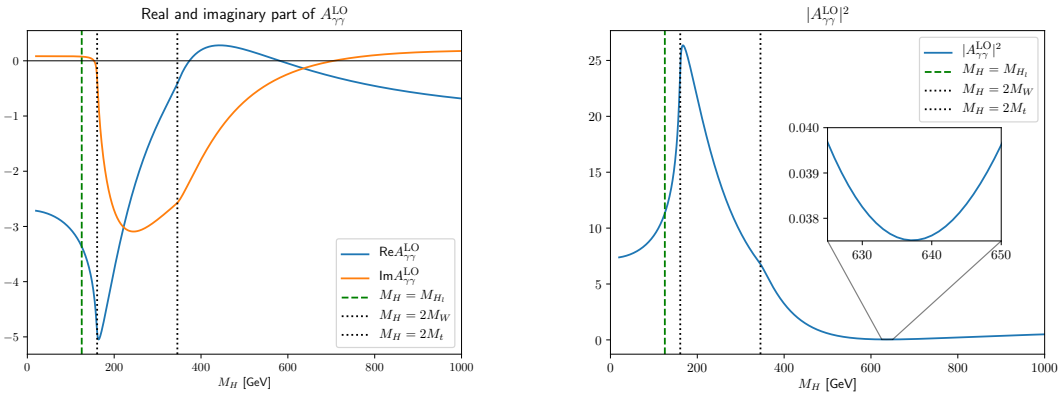

(a) (b)

Figure 2. The real and imaginary part of the full dimensionless amplitude $A_{\gamma\gamma}^{\rm LO}$ (left) and its squared modulus (right). The vertical dashed line denotes the location of the SM Higgs-boson $M_H = M_{H_l} = 125.25\,\text{GeV}$. The vertical dotted lines indicate the location of the WW- and $t\bar{t}$-thresholds. The dimensionless amplitudes are evaluated with complex masses as described in section 3.2.

HSESM through gluon fusion is given by

$$\begin{aligned}\sigma_{\rm HSESM}^{\rm LO}(g+g\to H) &= \frac{G_F M_H^2 \alpha_s^2}{128\sqrt{2}\pi}\, c_H^2\, |A_{gg}^{\rm LO}|^2\, \delta(s-M_H^2)\\ &= \hat{\sigma}^{\rm LO}\, M_H^2\, \delta(s-M_H^2)\,,\end{aligned} \tag{3.7}$$

with the strong coupling constant α_s and the dimensionless amplitude $A_{gg}^{\rm LO} = A_{\rm top}(\tau_t)$ from eq. (3.4). We consider again only the top-quark as a massive fermion and all other quarks as massless. Likewise the partial decay width for the Higgs-boson decay into two gluons is given by

$$\Gamma_{\rm HSESM}^{\rm LO}(H\to g+g) = \frac{G_F M_H^3 \alpha_s^2}{16\sqrt{2}\pi^3}\, c_H^2\, |A_{gg}^{\rm LO}|^2\,. \tag{3.8}$$

For the inclusion of the NLO electroweak corrections we write the dimensionless amplitudes as

$$A_z = A_z^{(1)} + g_W^2 A_z^{(2)} + \mathcal{O}(g_W^4), \qquad g_W^2 = \frac{G_F M_W^2}{8\sqrt{2}\pi^2}\,, \tag{3.9}$$

where z denotes the process, either $z=\gamma\gamma$ or $z=gg$. The one-loop LO dimensionless amplitude is given by $A_z^{(1)} \equiv A_z^{\rm LO}$ and similarly $A_z^{(2)}$ is the two-loop dimensionless amplitude containing the electroweak corrections. The NLO electroweak percentage corrections $\delta_{\rm EW}$ are then given by

$$|A_z|^2 = \left|A_z^{(1)}\right|^2 (1+\delta_{\rm EW})\,, \qquad \text{with} \qquad \delta_{\rm EW} = \frac{2\,\mathrm{Re}[g_W^2 A_z^{(2)} A_z^{(1)\dagger}]}{|A_z^{(1)}|^2}\,. \tag{3.10}$$

Let us remark that in the determination of the electroweak percentage corrections of eq. (3.10) the overall factors of eq. (3.1) and (3.7) cancel for both processes; in particular

JHEP11(2023)113

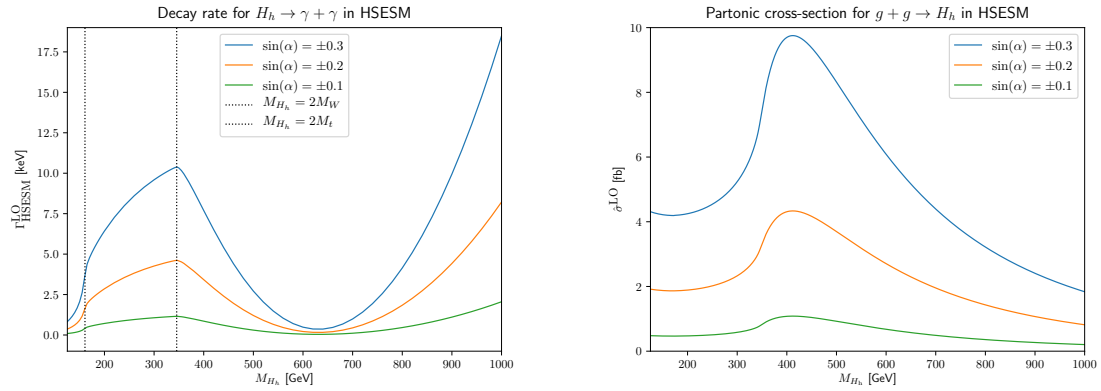

(a) (b)

Figure 3. Behaviour of the LO partial decay width for $H_h \to \gamma + \gamma$ (a) of eq. (3.1) and of the LO partonic cross-section $\hat{\sigma}_{\rm LO}$ for $g + g \to H_h$ (b) of eq. (3.7). The vertical dotted lines indicate the location of the WW- and $t\bar{t}$-thresholds.

the overall Higgs-boson mass dependence drops out. Hence $\delta_{\rm EW}$ as defined in eq. (3.10) describes the electroweak percentage corrections of the partial decay width and partonic cross section.

In figure 3 we show the LO partial decay width of eq. (3.1) for the process $H_h \to \gamma + \gamma$ as well as the partonic LO cross section $\hat{\sigma}^{\rm LO}$ of eq. (3.7) for the process $g + g \to H_h$ as a function of the heavy Higgs-boson mass for three different values of $\sin\alpha$ evaluated numerically with the input parameters of eqs. (3.6). For the process $g + g \to H_{\rm h}$ we use a running strong coupling constant α_s as implemented in the program `RunDec` [56]. In figure 3(a) one can see a clear maximum at $M_{H_{\rm h}} = 2M_t$ corresponding to the $t\bar{t}$-threshold of the top-triangle and a kink at $M_{H_{\rm h}} = 2M_W$, which corresponds to the WW-threshold present in the bosonic contribution of the process $H_{\rm h} \to \gamma + \gamma$.

3.2 Outline of the calculation

Feynrules [57, 58] was employed to generate all Feynman rules that are independent of gauge parameters, while the gauge-fixing vertices were implemented separately in the t'Hooft-Feynman gauge. All diagrams were generated using QGRAF [59] and the resulting expressions were manipulated using the in-house code QGS, which is based on FORM [60, 61]. Typical Feynman diagrams for the considered processes are depicted in figure 4. The program QGS is an extension of GraphShot(GS), already used for these same processes in the SM [41, 42]. QGS has been extended to work within the 2HDM [52, 53] and now the HSESM. The code, after performing the standard operations connected to the Dirac algebra with an anticommuting γ_5 (no anomalous diagrams are present for the processes under consideration), identifies the Lorentz structures of the amplitude by using projectors. This allows for a fast computation of the amplitude by only considering those Lorentz structures which enter in the squared amplitude of the physical process at the end of the calculation. In a next step the obtained expressions are simplified by removing reducible

JHEP11(2023)113

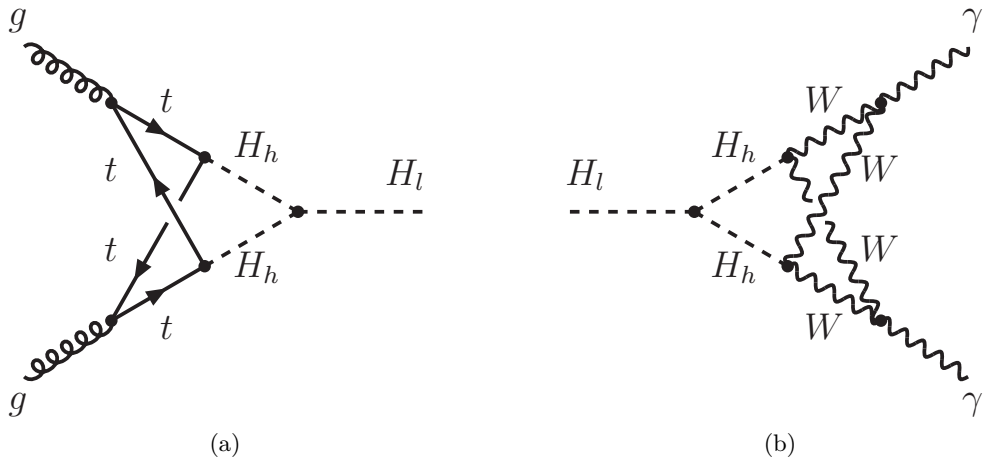

Figure 4. Two typical Feynman diagrams which contribute to our calculation of the NLO electroweak corrections to the Higgs-boson production through gluon fusion (a) and the Higgs-boson decay into two photons (b) are shown.

scalar products and using symmetries. This allows to reduce the amplitude to a combination of a small set of tensor integrals contracted with external momenta, which can be considered as the master integrals of the process under consideration. The UV-divergent part of these integrals is then extracted and canceled analytically against the analogous part of the counterterms, which do not depend on the specific renormalization scheme adopted. The inclusion of the finite part of the counterterms, which we call finite renormalizations, will be discussed in the next section 3.3. The obtained UV-finite amplitude still contains divergent integrals due to collinear singularities related to massless fermions. Since the electroweak corrections for both processes can not be divergent (there is no real emission which could compensate such singularities), we extract the divergent behaviour of each integral as logarithms in a small fictitious fermion mass and verify their cancellation analytically. The remaining loop integrals are then written in Feynman-parametric spaces in a form suited for numerical evaluation, following the techniques described in refs. [43, 62–64]. The integrands of the obtained integrals are then collected in a Fortran library and the whole amplitude is evaluated numerically with the desired numerical accuracy using an in-house integrator based on the Korobov-Conroy number theoretic methods [65–67]. Here we need to evaluate integrals up to dimension five numerically.

3.3 Renormalization

For the renormalization procedure of the SM parameters of the two processes $g + g \to H_{l,h}$ and $H_{l,h} \to \gamma + \gamma$ we proceed as follows. The renormalization of masses and wave-functions is done in the HSESM as in the SM, i.e. the related counterterms are written in terms of self-energies, but computed in the HSESM, getting expressions similar to those given in refs. [41, 43]. For the renormalization of G_F on the contrary we take directly the SM expression, assuming that contributions from the HSESM are negligible. For the renormalization of the W- and Z-boson masses as well as for the top-quark mass we use the

JHEP11(2023)113

complex mass scheme [68–70], where all parameters of the theory which depend on M_W, M_Z and M_t become complex.

Concentrating on the new parameters of the HSESM discussed in section 2, we see that they are the heavy Higgs-boson mass M_{H_h}, the ratio of the vevs $\tan\beta$ and the mixing angle α which are not present in the SM. For a complete renormalization of the HSESM, both α and β have to be renormalized in addition to M_{H_h}, for which we perform the on-shell renormalization. However, for the processes under consideration in this work, $\tan\beta$ does not appear at LO and it is sufficient to renormalize the mixing angle α.

On top of this we introduce additional counterterms in a tadpole scheme, in order to avoid the computation of diagrams with Higgs tadpoles attached. A $\overline{\mathrm{MS}}$ renormalization of the mixing angles of the HSESM requires a proper treatment of the Higgs tadpoles in order to obtain gauge-independent results for physical observables. The Fleischer-Jegerlehner(FJ)-tadpole scheme was introduced for a consistent treatment of the Higgs-tadpoles in the SM [71]. The FJ tadpole scheme in the SM is equivalent to the β_t scheme of ref. [72]. The FJ tadpole scheme has been extended for a general Higgs sector in ref. [51], which we apply here for the HSESM. Denoting the bare vevs, which minimize the bare scalar potential, with a superscript B, we write $v = v^B + \Delta v$, $v_S = v_S^B + \Delta v_S$ and get for the counterterms

$$\begin{aligned}
\Delta v = v\,\frac{G_F}{\pi^2\sqrt{8}}\Bigg\{ & \frac{1}{4}\left[\left(1-\frac{M_{H_l}^2}{M_{H_h}^2}\right)\left(s_\alpha^2\,c_\alpha^2 - \frac{s_\alpha^3 c_\alpha}{t_\beta}\right) - \frac{3}{2}\,c_\alpha^2\right] A_0(M_{H_l}) \\
& + \frac{1}{4}\left[\left(1-\frac{M_{H_h}^2}{M_{H_l}^2}\right)\left(s_\alpha^2\,c_\alpha^2 + \frac{s_\alpha c_\alpha^3}{t_\beta}\right) - \frac{3}{2}\,s_\alpha^2\right] A_0(M_{H_h}) \\
& - \frac{1}{8}\Big(2\,A_0(M_W) + A_0(M_Z)\Big) \\
& - \frac{c_\alpha^2\,M_{H_h}^2 + s_\alpha^2\,M_{H_l}^2}{M_{H_l}^2\,M_{H_h}^2}\Bigg[\frac{d-1}{4}\Big(2\,M_W^2\,A_0(M_W) + M_Z^2\,A_0(M_Z)\Big) \\
& \qquad - \sum_l M_l^2 A_0(M_l) - 3\sum_q M_q^2 A_0(M_q)\Bigg]\Bigg\}\,,
\end{aligned} \tag{3.11}$$

$$\begin{aligned}
\Delta v_S = v_S\,\frac{G_F}{\pi^2\sqrt{8}}\,\frac{1}{t_\beta}\Bigg\{ & \frac{1}{4}\left[\left(1-\frac{M_{H_l}^2}{M_{H_h}^2}\right)\left(\frac{s_\alpha^2\,c_\alpha^2}{t_\beta} - s_\alpha c_\alpha^3\right) - \frac{3}{2}\,\frac{s_\alpha^2}{t_\beta}\right] A_0(M_{H_l}) \\
& + \frac{1}{4}\left[\left(1-\frac{M_{H_h}^2}{M_{H_l}^2}\right)\left(\frac{s_\alpha^2 c_\alpha^2}{t_\beta} + s_\alpha^3\,c_\alpha\right) - \frac{3}{2}\,\frac{c_\alpha^2}{t_\beta}\right] A_0(M_{H_h}) \\
& - s_\alpha\,c_\alpha\,\frac{M_{H_h}^2 - M_{H_l}^2}{M_{H_l}^2\,M_{H_h}^2}\Bigg[\frac{d-1}{4}\Big(2\,M_W^2\,A_0(M_W) + M_Z^2\,A_0(M_Z)\Big) \\
& \qquad - \sum_l M_l^2 A_0(M_l) - 3\sum_q M_q^2 A_0(M_q)\Bigg]\Bigg\}\,,
\end{aligned} \tag{3.12}$$

where A_0 is the 1-point one-loop function and d are the space-time dimensions. In refs. [73, 74] a new scheme for tadpole renormalization, dubbed gauge-invariant vacuum expectation value scheme, was introduced being perturbatively stable. Its implementation is beyond the scope of the current work.

JHEP11(2023)113

A $\overline{\text{MS}}$ renormalization of mixing angles can lead to unnatural large corrections and can suffer from a large scale dependence. Within this work we focus on the renormalization schemes for the mixing angle α in the HSESM which were proposed in ref. [24] and proven to be gauge-parameter independent. In particular we discuss three schemes dubbed ZZ scheme, $\overline{\Psi}\Psi$ scheme and OS scheme in the following.[4]

First, the amplitudes for the decays of the two Higgs-bosons of the HSESM into two Z bosons were used in ref. [24] in order to define a physical renormalization scheme. At LO they read $\mathcal{M}^{(0)}_{H\to Z+Z} = -c_H M_W e/(s_W c_W^2)(\varepsilon_1^* \varepsilon_2^*)$, $(H = H_l \text{ or } H_h)$, where e is the elementary charge, $s_W(c_W)$ is the sine(cosine) of the weak mixing angle, ε_i $(i = 1, 2)$ are the two polarization vectors of the external Z bosons and c_H is defined in eq. (3.2). After all other parameters have been renormalized the renormalization condition for the mixing angle α requires that the ratio of the two amplitudes

$$\frac{\mathcal{M}_{H_h\to Z+Z}}{\mathcal{M}_{H_l\to Z+Z}} \stackrel{!}{=} -\frac{\sin(\alpha)}{\cos(\alpha)} \tag{3.13}$$

is equal to its LO value, where we have adapted the condition of ref. [24] to the definition of the mixing angle in eq. (2.4). Denoting bare quantities with a subscript B the bare mixing angle α_B is related to the renormalized one through the counterterm $\delta\alpha$ as $\alpha_B = \alpha + \delta\alpha$. Similarly, the bare and renormalized mass eigenstates of the heavy and light Higgs boson fields of eq. (2.4) are related by the renormalization constants δZ_{ij} $(i, j \in \{H_\text{l}, H_\text{h}\})$ through

$$\begin{pmatrix} H_{\text{h,B}} \\ H_{\text{l,B}} \end{pmatrix} = \begin{pmatrix} 1 + \frac{1}{2}\delta Z_{H_\text{h}H_\text{h}} & \frac{1}{2}\delta Z_{H_\text{h}H_\text{l}} \\ \frac{1}{2}\delta Z_{H_\text{l}H_\text{h}} & 1 + \frac{1}{2}\delta Z_{H_\text{l}H_\text{l}} \end{pmatrix} \begin{pmatrix} H_\text{h} \\ H_\text{l} \end{pmatrix}, \tag{3.14}$$

with

$$\delta Z_{H_\text{h}H_\text{l}} = \frac{2}{M^2_{H_\text{h}} - M^2_{H_\text{l}}} \Sigma_{H_\text{h}H_\text{l}}(M^2_{H_\text{l}}), \qquad \delta Z_{H_\text{l}H_\text{h}} = \frac{2}{M^2_{H_\text{l}} - M^2_{H_\text{h}}} \Sigma_{H_\text{h}H_\text{l}}(M^2_{H_\text{h}}), \tag{3.15}$$

where $\Sigma_{H_\text{h}H_\text{l}}$ is the Higgs mixing energy. Using the renormalization condition of eq. (3.13) the counterterm of the mixing angle can be written as [24]

$$\delta\alpha = c_\alpha s_\alpha \left(\delta_{H_l ZZ} - \delta_{H_h ZZ}\right) + \frac{1}{2} c_\alpha s_\alpha \left(\delta Z_{H_\text{l}H_\text{l}} - \delta Z_{H_\text{h}H_\text{h}}\right) - \frac{1}{2}\left(\delta Z_{H_\text{h}H_\text{l}} s_\alpha^2 - \delta Z_{H_\text{l}H_\text{h}} c_\alpha^2\right), \tag{3.16}$$

where $c_\alpha = \cos(\alpha)$, $s_\alpha = \sin(\alpha)$ and $\delta_{H_i ZZ}$ $(i \in \{l, h\})$ are the unrenormalized relative one-loop corrections to the two decays. In practical applications a choice of the polarization vectors has to be made. If one considers the amplitudes of these two decays at LO without the external polarization vectors ε_i, their Lorentz structure consists only of the metric tensor. Considering higher order corrections additional tensor structures arise, which depend on the external momenta. We have studied several physical renormalization schemes already in refs. [52, 53] in the context of the 2HDM, where also the Higgs boson decay into two Z bosons was considered in a renormalization condition. There we required as renormalization

[4] In ref. [24] the ZZ and $\overline{\Psi}\Psi$ schemes are described in section 3.2.1 and denoted as physical (on-shell) renormalization schemes, while our OS scheme is treated in section 3.3.1 and called rigid symmetry and wave-function renormalization for physical states.

JHEP11(2023)113

condition that the coefficient of the metric tensor in the above tensor decomposition of the amplitude is equal to its LO value. Similarly as in the 2HDM, we choose the polarization vectors of the external Z bosons here in the HSESM in such a way that all additional tensors vanish and only the form factor of the metric tensor survives. We will call this scheme ZZ scheme in the following.

A possible drawback of the ZZ scheme is that $\delta_{H_l ZZ}$ of eq. (3.16) has to be evaluated in the unphysical region, when H_l is identified with the observed Higgs state with a mass less than $2\,M_Z$. For this reason, a second renormalization scheme was defined in ref. [24] by adding a fermion singlet field Ψ to the field content of the HSESM and coupling it to the singlet scalar through a Yukawa coupling which is sent to zero in order to recover the original theory. As renormalization condition for the mixing angle α one considers here again the decays of the light and heavy Higgs bosons, this time into a pair of the new singlet fields Ψ, and again requires that the ratio of the two amplitudes is equal to its LO value in the limit of vanishing coupling:

$$\frac{\mathcal{M}_{H_h \to \Psi+\overline{\Psi}}}{\mathcal{M}_{H_l \to \Psi+\overline{\Psi}}} \stackrel{!}{=} \frac{\mathcal{M}^{(0)}_{H_h \to \Psi+\overline{\Psi}}}{\mathcal{M}^{(0)}_{H_l \to \Psi+\overline{\Psi}}}. \tag{3.17}$$

From this renormalization condition, the counterterm of the mixing angle α can be calculated to be [24]

$$\delta\alpha = -\frac{1}{2} c_\alpha s_\alpha \left(\delta Z_{H_\mathrm{l} H_\mathrm{l}} - \delta Z_{H_\mathrm{h} H_\mathrm{h}}\right) - \frac{1}{2}\left(\delta Z_{H_\mathrm{h} H_\mathrm{l}} c_\alpha^2 - \delta Z_{H_\mathrm{l} H_\mathrm{h}} s_\alpha^2\right). \tag{3.18}$$

This scheme will be denoted in the following as $\overline{\Psi}\Psi$ scheme. We note that, as opposed to the ZZ scheme, the counterterm of the $\overline{\Psi}\Psi$ scheme does not depend on the unrenormalized one-loop corrections of the defining decays. This is due to the fact that these vanish in the limit of vanishing Yukawa coupling.

The explicit counterterms for the mixing angle α for the above two schemes were already given in ref. [24], which we adapted to our conventions. A drawback of the ZZ and $\overline{\Psi}\Psi$ schemes is that they introduce artificial thresholds for the processes $g + g \to H_l$ and $H_l \to \gamma + \gamma$ when the heavy Higgs boson mass M_{H_h} is equal to twice the light Higgs boson mass M_{H_l}, as we will see explicitly in section 4. These thresholds originate from the wave function factor of the heavy Higgs boson, which enters the counterterm of the mixing angle through the decay amplitude of the heavy Higgs boson. Interestingly, the threshold singularities induced in this way, have opposite signs in the two schemes as can be seen from eqs. (3.16) and (3.18). This is due to the fact that in the ZZ scheme the couplings of the Higgs bosons to the Z bosons are induced by ρ_1, which couples to the gauge bosons, whereas in the $\overline{\Psi}\Psi$ scheme the couplings to the new fermions are induced by ρ_2. We call these thresholds here artificial, because they are absent in the pure two-loop amplitude, enter only throught the renormalization conditions from above and are absent in the last scheme for $\delta\alpha$ which is described in the next paragraph and which is free of this problem.

In the third and last scheme which we will consider in this paper the counterterm $\delta\alpha$ of the mixing angle α is fixed through the non-diagonal field renormalization constants of the

JHEP11(2023)113

light and heavy Higgs boson, avoiding the introduction of a threshold at $M_{H_\mathrm{h}} = 2M_{H_\mathrm{l}}$ in processes with a light external Higgs boson. The counterterm $\delta\alpha$ in this scheme is simply given by

$$\delta\alpha = \frac{\delta Z^{\mathrm{BFM}}_{H_\mathrm{h}H_\mathrm{l}} - \delta Z^{\mathrm{BFM}}_{H_\mathrm{l}H_\mathrm{h}}}{4}. \tag{3.19}$$

This renormalization condition has been introduced for the 2HDM and the HSESM in refs. [24, 75]. The authors of ref. [24] have proven the gauge independence of this scheme working in the background-field method (BFM), this means that $\delta Z^{\mathrm{BFM}}_{H_\mathrm{h}H_\mathrm{l}}$ and $\delta Z^{\mathrm{BFM}}_{H_\mathrm{l}H_\mathrm{h}}$ should be computed in the BFM. In our work we have computed the on-shell field renormalization constants of eq. (3.19) in the conventional formalism and then used the prescriptions described in appendix B of ref. [24] to translate them into the required BFM expressions. We then get

$$\begin{aligned}\delta\alpha = \frac{\delta Z_{H_\mathrm{h}H_\mathrm{l}} - \delta Z_{H_\mathrm{l}H_\mathrm{h}}}{4} - \frac{\alpha_{\mathrm{em}}\, c_\alpha\, s_\alpha}{32\pi c_W^2\, s_W^2}\Big\{ 2\, c_W^2 \Big[B_0(M^2_{H_\mathrm{h}}, M_W, M_W) - B_0(M^2_{H_\mathrm{l}}, M_W, M_W)\Big] \\ + B_0(M^2_{H_\mathrm{h}}, M_Z, M_Z) - B_0(M^2_{H_\mathrm{l}}, M_Z, M_Z)\Big\}\quad ,\end{aligned} \tag{3.20}$$

where B_0 is the scalar 2-point one-loop function. We will label this scheme in the following as on-shell(OS) scheme.

3.4 Checks

Several checks were performed to validate the set-up and the correctness of the computation. The UV- and tadpole renormalization procedures were validated by checking analytically that the amplitudes are UV-finite after renormalization. We implemented the FJ tadpole scheme for the HSESM and verified that the physical counterterms are independent of gauge parameters in a general R_ξ gauge. The finite renormalization was validated by checking that the dependence on the renormalization scale μ cancels in the three renormalization schemes described earlier in this section. The Feynman rules were checked by comparing the amplitudes for the processes $H_l \to Z + Z$, $H_h \to Z + Z$ and $H_h \to H_l + H_l$ as well as for $g + g \to H_l$, $g + g \to H_h$, $H_l \to \gamma + \gamma$ and $H_h \to \gamma + \gamma$ with Recola [22, 76] at LO and at NLO for the non loop-induced processes. The processes $H_l \to Z + Z$ and $H_h \to Z + Z$ were compared in the $\overline{\mathrm{MS}}$, OS and $\overline{\Psi}\Psi$ schemes, whereas the process $H_h \to H_l + H_l$ was checked in the $\overline{\mathrm{MS}}$ scheme only, since it requires additional renormalization of the parameter $\tan\beta$ in the other schemes. We checked that the amplitudes for the processes $H_l \to Z + Z$ and $H_h \to Z + Z$ fulfill indeed the renormalization condition of eq. (3.13) at NLO in the ZZ scheme. The appropriate IR behaviour of the amplitudes of the processes $g + g \to H_\mathrm{l}$, $H_\mathrm{l} \to \gamma + \gamma$, $g + g \to H_\mathrm{h}$ and $H_\mathrm{h} \to \gamma + \gamma$ was guaranteed by checking that the collinear singularities cancel as already described in section 3.2. Furthermore, for all four processes it was checked that the Ward identity, where we replace the external polarization vectors of the photons(gluons) by their momenta, is satisfied. For the processes $g + g \to H_\mathrm{l}$ as well as $H_\mathrm{l} \to \gamma + \gamma$ the corresponding amplitudes in the HSESM were found to agree analytically with the corresponding SM amplitudes in the SM limit of the HSESM. We checked our numerical integration by scaling all dimensionful quantities like masses and momenta by a

JHEP11(2023)113

BP	M_{H_h} [GeV]	$\sin(\alpha)$	$1/\tan(\beta)$
BHM200$\mp$	200	$\mp$0.29	1.19
BHM300$\mp$	300	$\mp$0.31	0.79
BHM400a$\mp$	400	$\mp$0.26	0.58
BHM400b	400	+0.26	0.59
BHM500a$\mp$	500	$\mp$0.24	0.46
BHM500b	500	+0.24	0.47
BHM600$\mp$	600	$\mp$0.22	0.38
BHM700a$\mp$	700	$\mp$0.21	0.31
BHM700b	700	+0.21	0.32
BHM800a$\mp$	800	$\mp$0.20	0.25
BHM800b	800	+0.20	0.27

Table 1. The benchmark points (BP) of refs. [37, 38] are shown in our conventions. The mass of the heavy Higgs boson is encoded in the BP's name. The BPs which have the same heavy Higgs-boson mass, but the name differs by the suffix a or b have the same (positive) value of $\sin\alpha$ and are distinguished by a tiny difference in the value of $\tan\beta$.

scaling parameter Λ for all four processes. This is a powerful check since, while the total amplitude must be independent on Λ, the individual integrals depend on the specific choice of it. We checked that the numerical value of the total amplitude is not affected by varying the scaling parameter.

4 Results and discussion

In this section, we present the numerical results of phenomenologically interesting scenarios for light and heavy Higgs-boson production in gluon fusion and for the Higgs-boson decays into two photons. First, we show various plots which describe the impact of the electroweak corrections in terms of the mass of the heavy Higgs boson M_{H_h} for different values of $\sin\alpha$ and $\tan\beta$. We do this scan in the OS renormalization scheme described in section 3.3, which we choose as our reference scheme, since it is process independent as requested in refs. [24, 77] and avoids potential artificial features of the processes underlying the $\overline{\Psi}\Psi$ and ZZ schemes. For the values of $\sin\alpha$ we consider the range of $[-0.3, +0.3]$ which roughly covers the region not yet excluded by the ATLAS studies of ref. [21]. For the ratio of the vevs we restrict our analysis to values smaller than $\tan\beta = 10$, where we expect the larger impact of the electroweak corrections. Finally for the heavy Higgs-boson mass we consider values up to 1 TeV in order not to enter the non-perturbative regime.

Furthermore we consider the benchmark points (BPs) of table 1. The BPs are taken from the LHC Higgs cross section working[5] group report [38] and were proposed originally in ref. [37]. We have adapted the input parameters of the BPs in table 1 to our conventions of section 2, i.e. in ref. [37] the mixing angle α has opposite sign and $\tan\beta$ is given by the reciprocal value compared to table 1.

[5]Some recent analysis may have excluded some BPs. For example the benchmark points BHM200$\mp$ seem to be slightly excluded by the analysis presented in [11]. They can however be taken as samples of the behaviour of the corrections in the nearby allowed parameter region.

JHEP11(2023)113

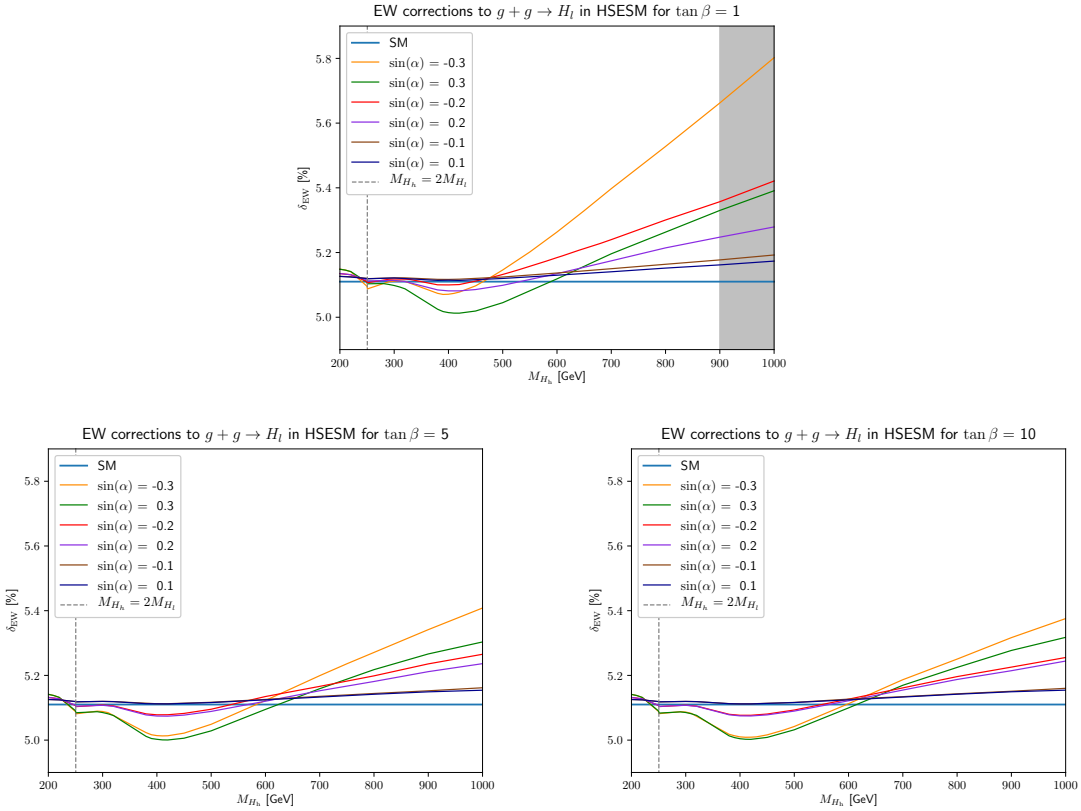

Figure 5. Relative NLO electroweak percentage corrections $\delta_{\rm EW}$ in the OS scheme to the LO cross section of the process $g + g \to H_l$ in the HSESM for $\tan\beta = 1, 5, 10$ with varying values of $\sin\alpha$. The SM limit is shown in blue.

Finally plots with the comparison of the three renormalization schemes for the mixing angle α are shown in dependence of the heavy Higgs-boson mass M_{H_h}, for specific values of $\sin\alpha$ and $\tan\beta$. First results in the ZZ-scheme were already presented in ref. [78]. For the numerical evaluation we use the input parameters given in eqs. (3.6). We use the complex mass scheme [68–70] for the renormalization of the W- and Z-boson masses as well as for the top quark mass. For the two processes which have the heavy Higgs boson as an external particle, i.e. for heavy Higgs-boson production in gluon fusion and for the heavy Higgs-boson decay into two photons, the light Higgs boson appears only as an internal particle and is thus also renormalized in the complex mass scheme.

4.1 Higgs-boson production in gluon fusion in the HSESM

Choosing as reference renormalization scheme for the mixing angle α the OS scheme as defined in section 3.3, we show in figure 5 the dependence of the electroweak percentage corrections $\delta_{\rm EW}$ defined in eq. (3.10) on M_{H_h} for the production of the light Higgs boson at 6 values of $\sin\alpha$ for each plot. The three plots of figure 5 are for the three values of $\tan\beta = 1, 5$ and 10.

JHEP11(2023)113

BP	$\delta_{\rm EW}$	BP	$\delta_{\rm EW}$	BP	$\delta_{\rm EW}$
BHM200−	5.2	BHM400b	5.0	BHM700a−	5.2
BHM200+	5.1	BHM500a−	5.1	BHM700a+	5.2
BHM300−	5.1	BHM500a+	5.1	BHM700b	5.2
BHM300+	5.1	BHM500b	5.1	BHM800a−	5.2
BHM400a−	5.1	BHM600−	5.1	BHM800a+	5.2
BHM400a+	5.0	BHM600+	5.1	BHM800b	5.2

Table 2. The electroweak percentage corrections $\delta_{\rm EW}$ [%] in the OS scheme are shown for the benchmark points of table 1 for the process $g + g \to H_1$.

The grey shaded area in the plot for $\tan\beta = 1$ indicates the onset of the non-perturbative regime, where at least one of the parameters $\frac{\lambda_i}{4\pi}$ ($i = 1, 2$ or 3) of eq. (2.1) becomes larger than one. This only happens for small values of $\tan\beta$, since the latter appears in the denominator of eqs. (2.8) and (2.9). The vertical dashed line indicates the location where the heavy Higgs-boson mass is twice the light Higgs-boson mass. All three plots of figure 5 show the same numerical range for the percentage correction and the heavy Higgs-boson mass in order to allow for a better comparison of the results for the three different values of $\tan\beta$. The electroweak corrections are very close to the ones in the SM (blue line), in the range of $5.0\% - 5.8\%$, showing the largest deviations at high values of M_{H_h}, small values of $\tan\beta$ and large absolute values of $\sin\alpha$. The behaviour of $\delta_{\rm EW}$ shows a small minimum around $M_{H_h} \approx 400\,\text{GeV}$ and grows almost linearly afterwards in the considered mass range. For $\tan\beta = 1$ the corrections are a little more enhanced than at $\tan\beta = 5$ and remain basically unchanged at larger values of $\tan\beta$. An interesting feature which we derive from the plots is the negligible dependence of the electroweak corrections on the sign of $\sin\alpha$ for large values of $\tan\beta$, revealing that the odd contributions in $\sin\alpha$ are $\tan\beta$-suppressed. This can be seen best in the last plot of figure 5 (for $\tan\beta = 10$) where the lines for $\pm\sin\alpha$ approach each other and almost coincide. This feature can also be verified by inspecting the analytical expressions for the corrections.

For the BPs of table 1 we show the electroweak percentage corrections in table 2 for the process $g + g \to H_1$. The mixing angle α has been renormalized in the OS scheme. All BPs are very close to the SM result of 5.1%, which is also shown by the blue line in figures 5 and 7. For high values of the heavy Higgs boson mass (larger than 600 GeV) one can see a small increase of the percentage correction compared to the SM result. Considering BPs with a heavy Higgs-boson mass close to the minimum of figure 5 one can also see here a small decrease of the percentage correction.

The electroweak percentage corrections which are provided in figure 5 and table 2 also apply to the partial decay width of the process $H_1 \to g + g$, since the amplitude A_{gg} which enters the partial decay width in eq. (3.8) as well as the amplitude A_{gg} which enters the cross section $\hat{\sigma}$ of eq. (3.7) are identical for both observables at leading order and only the global factor in front of the squared amplitude needs to be adjusted. This holds not only at leading order, but also at next-to-leading order when considering the electroweak corrections.

The same plots for the production of the heavy Higgs boson are shown in figure 6, which features larger (negative) electroweak percentage corrections compared to the production of the light Higgs boson. The axis of ordinates shows again the electroweak percentage

JHEP11(2023)113

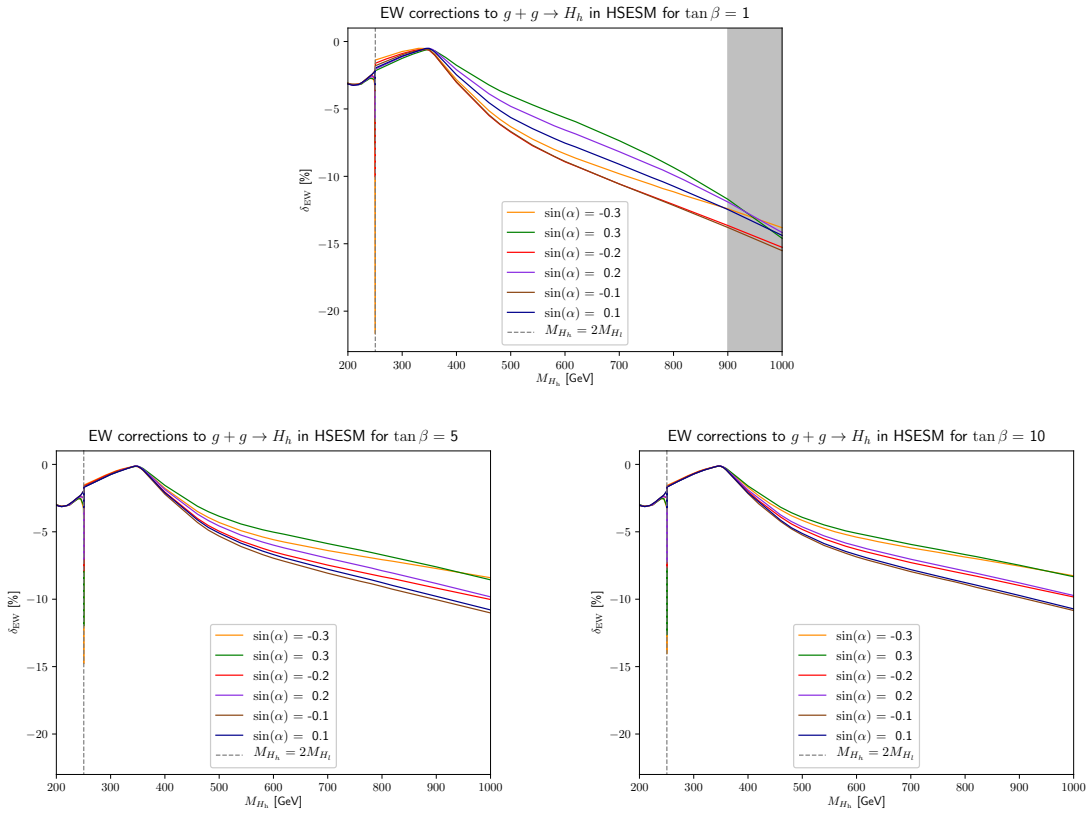

Figure 6. Relative NLO electroweak percentage corrections $\delta_{\rm EW}$ in the OS scheme to the LO partonic cross section of the process $g + g \to H_h$ in the HSESM for $\tan\beta = 1, 5, 10$ with varying values of $\sin\alpha$.

correction $\delta_{\rm EW}$ as a function of the heavy Higgs-boson mass $M_{H_{\rm h}}$ on the abscissa. Both axes show the same range of values for all three plots. Starting from around -3% for $M_{H_{\rm h}} \approx 200\,\text{GeV}$, the electroweak percentages corrections $\delta_{\rm EW}$ increase to a maximum close to $\delta_{\rm EW} \approx 0\%$ around $M_{H_{\rm h}} \approx 350\,\text{GeV}$ and decrease then almost linearly to reach $\delta_{\rm EW} \approx -15\%$ for $M_{H_{\rm h}} \approx 1000\,\text{GeV}$ (and $\tan\beta = 1$). We see again a comparable behaviour for $\tan\beta = 5$ and $\tan\beta = 10$, while the corrections are more sizable for $\tan\beta = 1$. Also for the production of a heavy Higgs boson we see that the electroweak corrections are basically independent of the sign of $\sin\alpha$ for large $\tan\beta$.

For the production of a heavy Higgs boson $H_{\rm h}$ we observe in figure 6 cusps for a heavy Higgs-boson mass of $M_{H_h} = 2M_{H_l}$. These cusps are threshold singularities which arise from the external heavy Higgs-boson wave function renormalization factor. Such threshold singularities of the processes considered here have been analyzed in detail in the SM in ref. [79]. Here, these singularities are regularized in the complex mass scheme by the complex light Higgs-boson mass and are thus finite. Since the total decay width of the light Higgs-boson is, however, very small, see eq. (3.6), the cusps do not completely disappear and remain visible in the electroweak percentage corrections.[6]

[6]We do not evaluate in detail the impact of the corrections in the threshold region, since they largely depend on the measured value of the total decay width of the light Higgs-boson, which is not yet precise enough to make a meaningful prediction in that region.

JHEP11(2023)113

BP	$\delta_{\rm EW}$	BP	$\delta_{\rm EW}$	BP	$\delta_{\rm EW}$
BHM200−	−3.1	BHM400b	−1.7	BHM700a−	−7.6
BHM200+	−3.1	BHM500a−	−5.2	BHM700a+	−6.9
BHM300−	−0.7	BHM500a+	−4.2	BHM700b	−6.9
BHM300+	−1.1	BHM500b	−4.2	BHM800a−	−8.2
BHM400a−	−2.3	BHM600−	−6.7	BHM800a+	−7.9
BHM400a+	−1.7	BHM600+	−5.8	BHM800b	−7.9

Table 3. The electroweak percentage corrections $\delta_{\rm EW}$ [%] in the OS scheme are shown for the benchmark points of table 1 for the process $g + g \to H_{\rm h}$.

For the BPs of table 1 we show the electroweak percentage corrections in table 3 for the process $g + g \to H_{\rm h}$. The mixing angle α has been renormalized in the OS scheme. For these BPs the percentage correction is always negative and follows the shape of the plots of figure 6. For Higgs-boson masses going from 200 GeV to 300 GeV, $\delta_{\rm EW}$ increases reaching a maximum close to zero for the benchmark point BHM300. For BPs with a larger value of the heavy Higgs-boson mass the electroweak percentage corrections decrease, i.e. they become large and negative.

The electroweak percentage corrections which we provide in figure 6 and table 3 also apply to the partial decay width of the process $H_{\rm h} \to g + g$ for the same reason as already discussed previously for the partial decay with of the process $H_{\rm l} \to g + g$.

Now we want to compare the three renormalization schemes under consideration, i.e. the OS scheme, the $\overline{\Psi}\Psi$ scheme and the ZZ scheme as introduced in section 3.3. In figure 7 we report the corrections for the light Higgs-boson production for $\sin\alpha = \pm 0.1$ and ± 0.3. We consider only $\tan\beta = 1$ and 10, since the behaviour for $\tan\beta = 5$ is similar to the one for $\tan\beta = 10$ in all renormalization schemes. For large values of $\tan\beta$ we show just the behaviour for negative $\sin\alpha$, since the corrections are essentially even in $\sin\alpha$ in this case, i.e. independent of the sign of $\sin\alpha$.

The electroweak corrections remain stable (and close to the SM) for small values of $\sin\alpha$, however, it can be seen that the ZZ scheme is slightly shifted upwards from the SM line for the whole range of heavy Higgs-boson masses under consideration. This feature is even enhanced for $\sin\alpha = \pm 0.3$. In particular for $\sin\alpha = -0.3$ large differences between the ZZ scheme and the other two schemes exist and the ZZ scheme shows a large dependence on the heavy Higgs-boson mass M_{H_h}, which enhances the correction at large M_{H_h} values. For $\tan\beta = 1$, going from negative $\sin\alpha = -0.3$ to positive $\sin\alpha = +0.3$, the percentage correction of the $\overline{\Psi}\Psi$ scheme is shifted upwards by approximately the same amount as the OS scheme is shifted downwards. Fixing instead now $\sin\alpha = -0.3$ and going from $\tan\beta = 1$ to $\tan\beta = 10$ the $\overline{\Psi}\Psi$ scheme is shifted downwards stronger than the OS scheme. Since for large $\tan\beta$ the corrections are insensitive to the sign of $\sin\alpha$, the corrections for $\tan\beta = 10$ and $\sin\alpha = -0.3$ are comparable to the corrections for $\tan\beta = 10$ and $\sin\alpha = +0.3$. Thus the shift in the $\overline{\Psi}\Psi$ scheme is even larger when going from $\tan\beta = 1$ to $\tan\beta = 10$ for the positive value of $\sin\alpha = +0.3$. Hence the $\overline{\Psi}\Psi$ scheme displays a stronger dependence on $\tan\beta$ than the OS scheme. The difference in the three schemes is the renormalization of the

JHEP11(2023)113

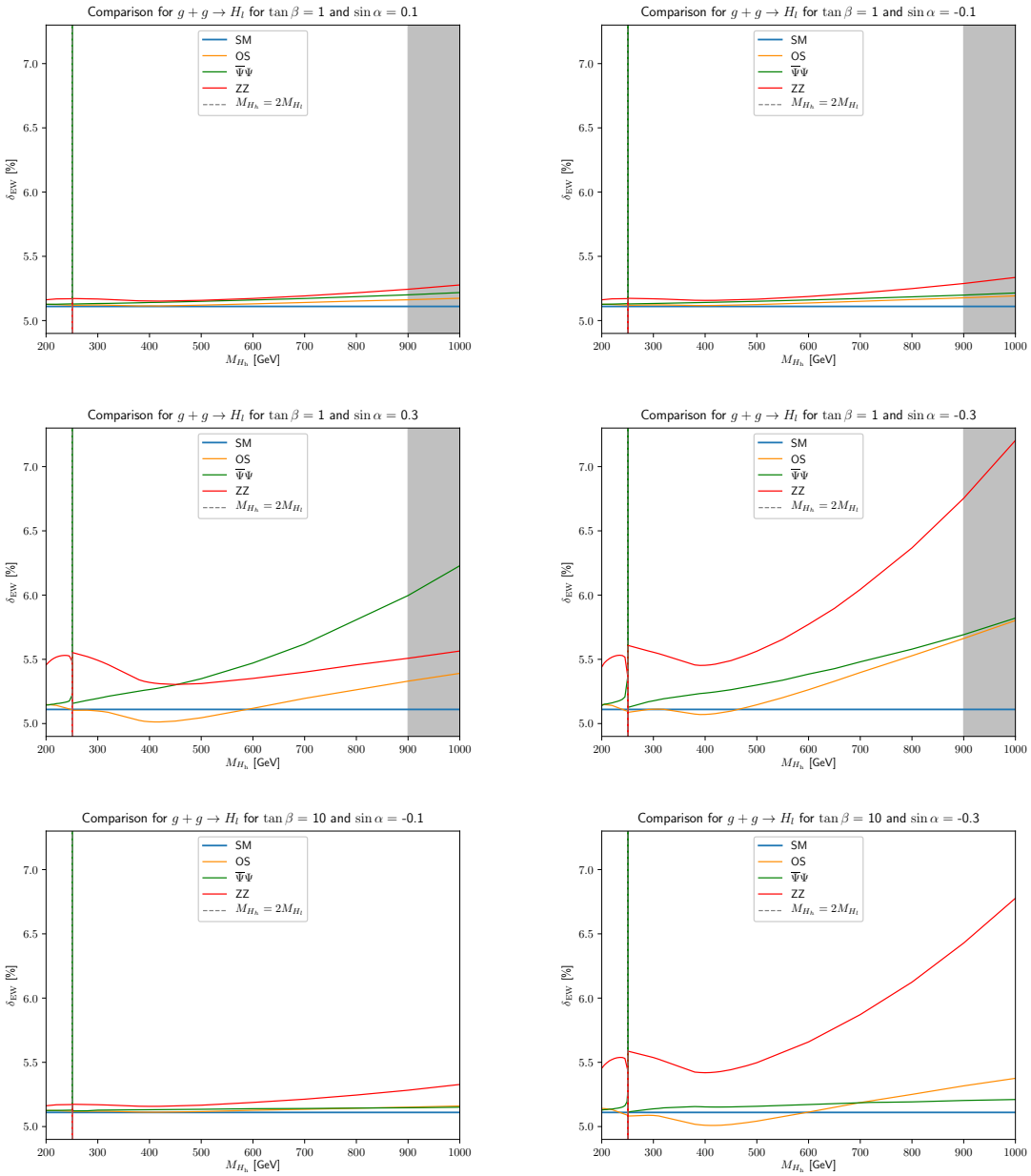

Figure 7. Comparison of the renormalization schemes for $g+g \to H_l$ in the HSESM for $\tan\beta = 1, 10$ with varying values of $\sin\alpha$. The SM limit is shown in blue.

JHEP11(2023)113

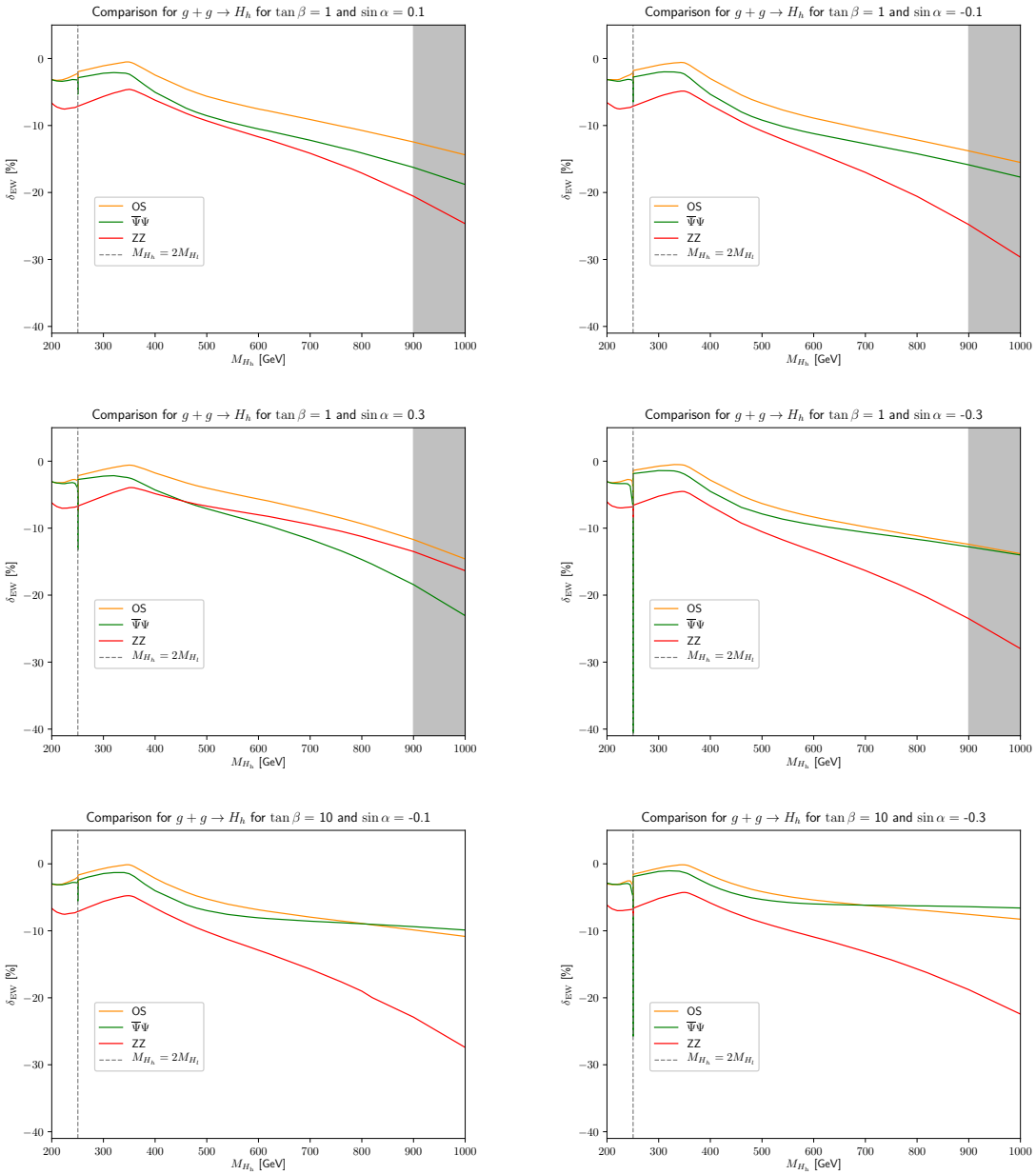

Figure 8. Comparison of the renormalization schemes for $g+g \to H_h$ in the HSESM for $\tan\beta = 1, 10$ with varying values of $\sin\alpha$.

JHEP11(2023)113

mixing angle α as shown by the explicit expressions for the counterterm $\delta\alpha$ in section 3.3. A peculiarity of the ZZ scheme is that its counterterm $\delta\alpha$ of eq. (3.16) has an additional term, $c_\alpha s_\alpha \left(\delta_{H_l ZZ} - \delta_{H_h ZZ}\right)$, which incorporates the information about the amplitudes of the processes $H_l \to Z + Z$ and $H_h \to Z + Z$. Such a term is absent in the $\overline{\Psi}\Psi$ and OS schemes of eqs. (3.18) and (3.19), causing the overall shift of the percentage correction in the ZZ scheme compared to the other schemes as well as its stronger M_{H_h} dependence (for negative values of $\sin\alpha$). Furthermore, both the counterterm corresponding to the $\overline{\Psi}\Psi$ scheme and the ZZ scheme depend on all Higgs field strength renormalization factors of eq. (3.14), whereas the counterterm corresponding to the OS scheme only depends on the off-diagonal ones. Since the $\tan\beta$ dependence originates from the trilinear Higgs couplings, the presence of the additional diagonal field strength renormalization factors in the $\overline{\Psi}\Psi$ scheme and the ZZ scheme introduces also an additional $\tan\beta$ dependence.

For the process of light Higgs-boson production there is no physical threshold singularity at $M_{H_h} = 2M_{H_l}$. As a result of this there are no cusps in figure 5 in the OS scheme, but only a small kink is visible for $M_{H_h} = 2M_{H_l}$. Analyzing figure 7 we observe for the ZZ and $\overline{\Psi}\Psi$ schemes that also for the process $g + g \to H_\mathrm{l}$ threshold singularities appear for $M_{H_h} = 2M_{H_l}$. These threshold singularities are introduced artificially through the two process dependent renormalization schemes as already mentioned in section 3.3. Both schemes rely on processes, where the decay of a heavy Higgs-boson enters, i.e. $H_\mathrm{h} \to Z + Z$ for the ZZ scheme and $H_\mathrm{h} \to \Psi + \overline{\Psi}$ for the $\overline{\Psi}\Psi$ scheme. In these two processes the heavy Higgs-boson wave function factor, which contains the threshold singularity, enters again. Thus these two schemes introduce the threshold singularities artificially into the process $g + g \to H_\mathrm{l}$, which are regularized in the complex mass scheme by the complex light Higgs-boson mass and are thus finite, but remain visible as artificial cusps. The OS-scheme is free of this drawback.

The dependence on the renormalization scheme for the heavy Higgs-boson production in gluon fusion is shown in figure 8. The results in the ZZ scheme appear shifted compared to the OS scheme, being always at least 4% different. The reason for this shift is again the first term of eq. (3.16) as already described in the discussion of the light Higgs-boson production in gluon fusion earlier in this section. For negative values of $\sin\alpha$ the ZZ scheme shows in addition a strong dependence on the heavy Higgs-boson mass, arriving at differences of the order of 15% for $M_{H_h} = 1000\,\mathrm{GeV}$ between the ZZ scheme and the other schemes. Going for the fixed value of $\tan\beta = 1$ from negative $\sin\alpha = -0.3$ to positive $\sin\alpha = +0.3$, the percentage correction of the $\overline{\Psi}\Psi$ scheme is shifted downwards by approximately the same amount as the ZZ scheme is shifted upwards. For large values of $|\sin\alpha| = 0.3$ the $\overline{\Psi}\Psi$ scheme shows again a stronger dependence on $\tan\beta$ than the other schemes. In all three schemes the EW percentage corrections have a maximum between $M_{H_\mathrm{h}} = 300\,\mathrm{GeV}$ and $M_{H_\mathrm{h}} = 400\,\mathrm{GeV}$, but the precise location and its shape are scheme dependent. In figure 8 one can see the threshold singularities for $M_{H_h} = 2M_{H_l}$, which are present in the plots for all schemes as expected. They are again regularized in the complex mass scheme by the complex light Higgs-boson mass and are thus finite, but remain as cusps since the width of the light Higgs boson is very small. The depth of the cusp caused by this threshold is strongly scheme dependent, with a deep cusp in the $\overline{\Psi}\Psi$ scheme and a hardly

JHEP11(2023)113

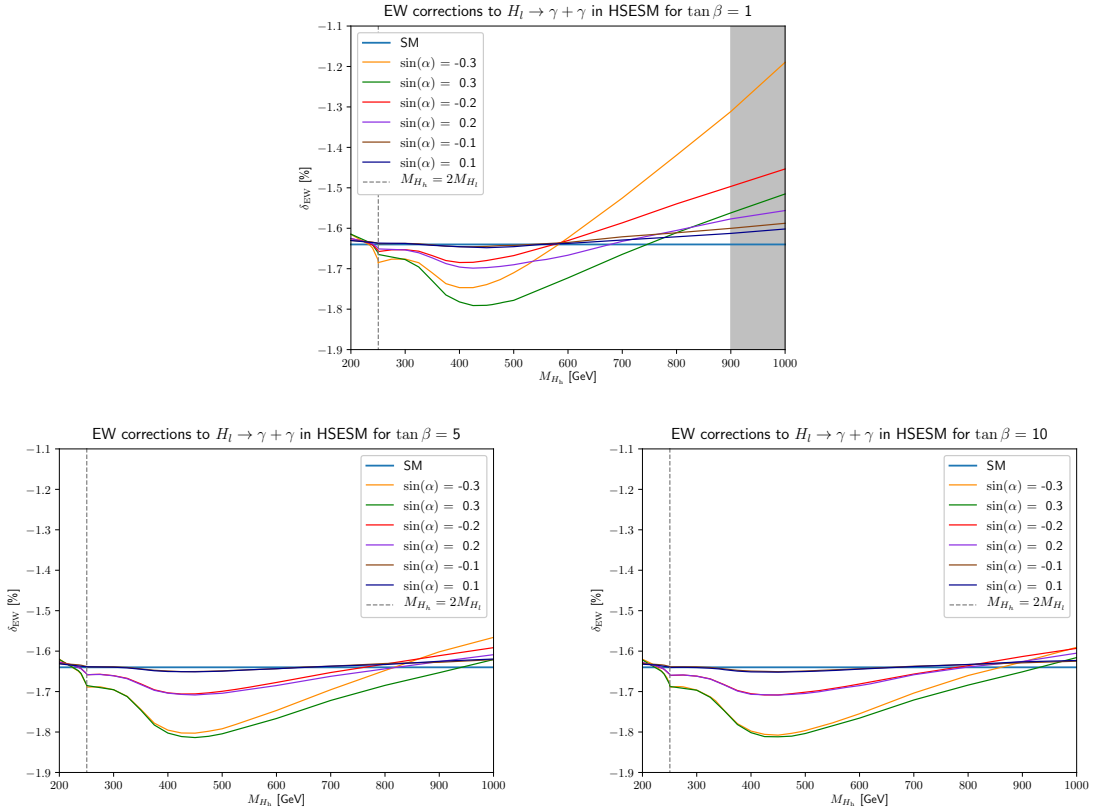

Figure 9. NLO electroweak percentage corrections $\delta_{\rm EW}$ in the OS scheme relative to the LO partial decay width of the process $H_l \to \gamma + \gamma$ in the HSESM for $\tan\beta = 1, 5, 10$ with varying values of $\sin\alpha$. The SM limit is shown in blue.

visible one in the ZZ scheme. The cusp originates from the field renormalization constant $\delta Z_{H_{\rm h}H_{\rm h}}$, which behaves around the threshold like $(1 - M^2_{H_{\rm h}}/(4M^2_{H_{\rm l}}))^{-1/2}$ and enters the renormalized amplitude directly through the wave function renormalization of the external heavy Higgs boson and indirectly through the renormalization of $\delta\alpha$. This second source arises, however, only for the ZZ- and $\overline{\Psi}\Psi$-scheme according to eq. (3.16) and eq. (3.18) respectively. Collecting these two sources of the cusp behaviour, we have that in the ZZ-, $\overline{\Psi}\Psi$-, and OS-scheme the electroweak percentage corrections $\delta_{\rm EW}$ depends on $\delta Z_{H_{\rm h}H_{\rm h}}$ like $(1 - c^2_\alpha)\delta Z_{H_{\rm h}H_{\rm h}}/2$, $(1 + c^2_\alpha)\delta Z_{H_{\rm h}H_{\rm h}}/2$, and $\delta Z_{H_{\rm h}H_{\rm h}}/2$ respectively. Since c^2_α is very close to 1 for $|\sin\alpha| \leq 0.3$, we see a cancellation in the coefficient of the cusp for the ZZ-scheme and an enhancement of it for the $\overline{\Psi}\Psi$-scheme, explaining the observed behaviour.

4.2 Higgs-boson decay into two photons in the HSESM

In this section we present results for the light and heavy Higgs-boson decay into two photons. Like in section 4.1 for the Higgs-boson production in gluon fusion, we choose also here for the Higgs-boson decay into two photons the OS scheme as defined in section 3.3 as reference renormalization scheme for the mixing angle α.

JHEP11(2023)113

BP	$\delta_{\rm EW}$	BP	$\delta_{\rm EW}$	BP	$\delta_{\rm EW}$
BHM200−	−1.6	BHM400b	−1.8	BHM700a−	−1.7
BHM200+	−1.6	BHM500a−	−1.7	BHM700a+	−1.7
BHM300−	−1.7	BHM500a+	−1.8	BHM700b	−1.7
BHM300+	−1.7	BHM500b	−1.8	BHM800a−	−1.6
BHM400a−	−1.7	BHM600−	−1.7	BHM800a+	−1.6
BHM400a+	−1.8	BHM600+	−1.7	BHM800b	−1.6

Table 4. The electroweak percentage corrections $\delta_{\rm EW}$ [%] for the decay process $H_{\rm l} \to \gamma + \gamma$ are shown for the benchmark points of table 1 for the mixing angle α in the OS scheme.

In figure 9 we show the electroweak percentage corrections $\delta_{\rm EW}$ defined in eq. (3.10) as a function of the heavy Higgs-boson mass $M_{H_{\rm h}}$ for the decay of a light Higgs boson for 6 values of $\sin\alpha$. The three plots of figure 9, for the three values of $\tan\beta = 1, 5$ and 10, show again the same numerical range for the percentage correction and the heavy Higgs-boson mass in order to allow to better compare the results for the three different values of $\tan\beta$. The SM result is again shown as the solid horizontal blue line in each plot. The electroweak corrections are negative and very close to the SM case. They range between about −1.8% to about −1.2% and are thus hardly to distinguish from the SM case. The largest deviations from the SM result can be observed again for high values of $M_{H_{\rm h}}$, small values of $\tan\beta$ and large absolute values of $\sin\alpha$. Similarly to light Higgs-boson production in gluon fusion of section 4.1 the electroweak percentage corrections $\delta_{\rm EW}$ for the light Higgs-boson decay into two photons shows also here a minimum between around $M_{H_{\rm h}} \approx 400 - 500\,\text{GeV}$. For the small value of $\tan\beta = 1$ in the first plot of figure 9 the different lines for the various values of $\sin\alpha$ differ more from each other than for larger values of $\tan\beta = 5, 10$, where the dependence of the electroweak corrections on the sign of $\sin\alpha$ becomes again negligible due to the $\tan\beta$-suppression already discussed in the previous section 4.1. This can be seen best again in the last plot of figure 9 (for $\tan\beta = 10$), where the lines for $\pm\sin\alpha$ approach each other and almost coincide.

For the BPs of table 1 we show the electroweak percentage corrections for the process $H_{\rm l} \to \gamma + \gamma$ in table 4, where the mixing angle α has been renormalized in the OS scheme. The corrections are very close to the result of the SM and follow the shape of the plots in figure 9 with a slight minimum around $M_{H_{\rm h}} \approx 400 - 500\,\text{GeV}$.

The electroweak percentage corrections for the heavy Higgs-boson decay into two photons in the HSESM are shown in figure 10 in three plots as a function of the heavy Higgs-boson mass $M_{H_{\rm h}}$. The three plots are again for the three values of $\tan\beta = 1$, 5, 10 and show the six values of $\sin\alpha = \pm0.1, \pm0.2, \pm0.3$. All three plots cover again the same range for the heavy Higgs-boson mass and the electroweak percentage correction, which allows to compare the three scenarios. While the electroweak percentage corrections for small heavy Higgs-boson masses around 200–300 GeV are only of the order of a few percent, they range from about −80% to about +40% for heavy Higgs-boson masses around 600 GeV and can thus become very large. Due to the wide range from large positive to large negative electroweak corrections, the different curves for the different values of $\sin\alpha$ are hard to distinguish.

JHEP11(2023)113

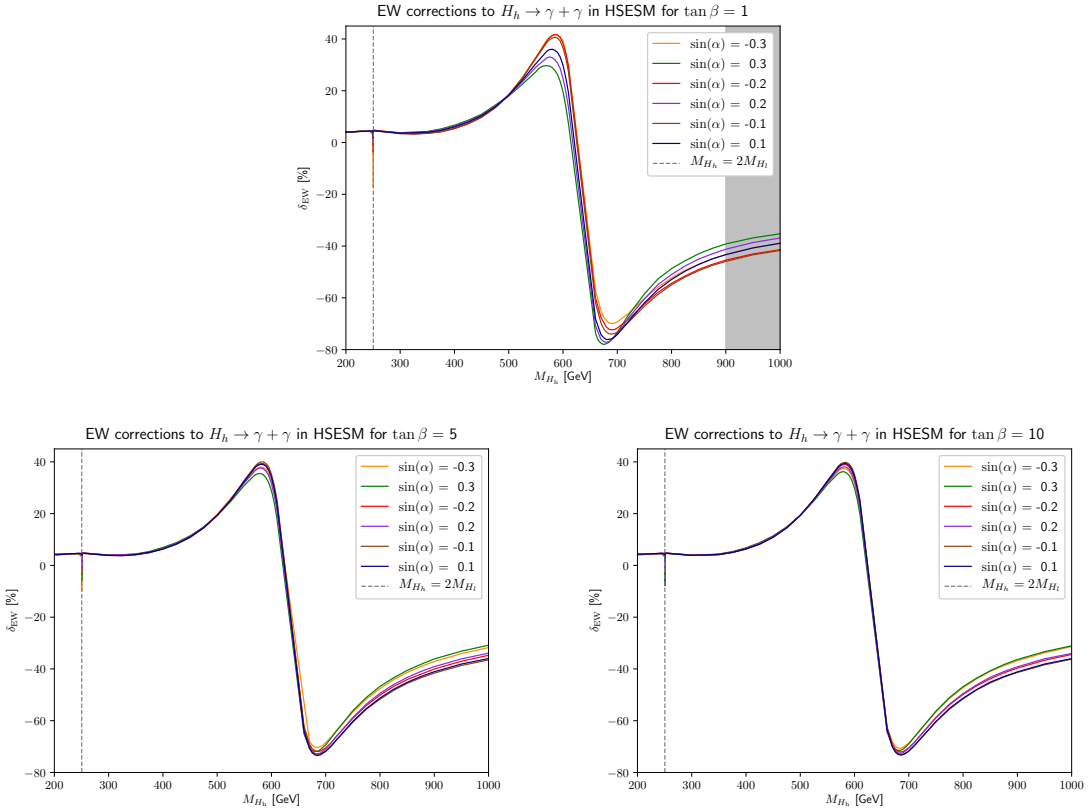

Figure 10. NLO electroweak percentage corrections $\delta_{\rm EW}$ relative to the LO partial decay width of the process $H_h \to \gamma + \gamma$ in the HSESM for $\tan\beta = 1, 5, 10$ with varying values of $\sin\alpha$. The mixing angle α is renormalized in the OS scheme.

The electroweak corrections have a maximum of 30% to 42% for a heavy Higgs-boson mass between 570 GeV and 585 GeV, a turning point for a heavy Higgs-boson mass of $M_{H_{\rm h}} \approx 630\,\text{GeV}$ and reach a minimum of -70% to -78% for a heavy Higgs-boson mass in the range of 675 GeV to 690 GeV. The exact size and location of the extrema depend on $\tan\beta$ and $\sin\alpha$. Again, for a small value of $\tan\beta = 1$ the curves for different values of $\sin\alpha$ are further apart than for large values of $\tan\beta = 5, 10$, where the curves with identical $|\sin\alpha|$ approach each other and essentially coincide for $\tan\beta = 10$ due to the $\tan\beta$-suppression. For $\tan\beta = 1$ the maximum for $\sin\alpha = -0.3$ is located at $M_{H_{\rm h}} = 585\,\text{GeV}$ with a value of around 42%, whereas the maximum for $\sin\alpha = +0.3$ is located at $M_{H_{\rm h}} = 570\,\text{GeV}$ with a value of around 30%. The location and size of the minimum behave in a similar way with the minimum of -70% being located at $M_{H_{\rm h}} = 690\,\text{GeV}$ for $\tan\beta = 1$ and $\sin\alpha = -0.3$ and the minimum of -78% being located at $M_{H_{\rm h}} = 675\,\text{GeV}$ for $\tan\beta = 1$ and $\sin\alpha = +0.3$.

The reason for the fast change from large positive to large negative corrections within a few GeV of the heavy Higgs-boson mass can be understood when taking into account figure 2(b), where the squared modulus of the LO amplitude $|A^{\rm LO}_{\gamma\gamma}|^2$ is shown. There the squared modulus of the amplitude strongly decreases for Higgs-boson masses larger than about 300 GeV and reaches a minimum between 630–640 GeV, where the squared modulus

JHEP11(2023)113

becomes almost zero. After the minimum it increases only slightly (see inset of figure 2(b)), but stays close to zero. The electroweak percentage corrections $\delta_{\rm EW}$ of figure 10 being according to eq. (3.10) an interference between the LO and NLO amplitude normalized to the squared modulus of the LO amplitude inherit this feature from the LO amplitude in the form of a large enhancement factor. In fact, the real and imaginary parts of the pure two-loop amplitude only change moderately for Higgs-boson masses between 600–700 GeV. However, the LO-NLO interference is such that it changes sign in this region. This change of sign paired with the large enhancement leads to a very sharp drop. Essentially we conclude that, even if $\delta_{\rm EW}$ is large in this region, we can not say that we are facing a breakdown of the perturbative expansion, but rather an accidental enhancement of the NLO electroweak corrections due to the smallness of the leading order amplitude. A similar behaviour, even more pronounced, was observed for the electroweak corrections to the Higgs-boson decay into two photons in the SM with a fourth generation of heavy fermions [50]. Because of this particular feature, to better illustrate the impact of electroweak corrections, we show the LO and NLO partial decay width for $H_h \to \gamma + \gamma$ in figure 11. For all considered values of $\tan\beta$ we observe at NLO a small shift to higher Higgs-boson masses of the LO minimum, after which the NLO corrections are sizable. The dependence of the decay rate on the sign of $\sin\alpha$ is very small for $\tan\beta = 1$ and essentially invisible for $\tan\beta = 5, 10$.

In figure 10 we observe again a cusp for a heavy Higgs-boson mass of $M_{H_{\rm h}} = 2M_{H_{\rm l}}$, this time also for a renormalization of the mixing angle α in the OS scheme. The cusp at the threshold of $M_{H_{\rm h}} = 2M_{H_{\rm l}}$ originates from the heavy Higgs-boson wave function factor. This threshold is here in this process $H_{\rm h} \to \gamma + \gamma$ a real physical threshold and not introduced artificially due to the choice of the renormalization scheme, like for the processes $g + g \to H_{\rm l}$ and $H_{\rm l} \to \gamma + \gamma$ in the ZZ or $\overline{\Psi}\Psi$ schemes. This threshold singularity is here again regularized by the complex mass of the light Higgs boson and is thus finite.

For the BPs of table 1 we show the electroweak percentage corrections in table 5 for the process $H_{\rm h} \to \gamma + \gamma$. The mixing angle α is renormalized in the OS scheme. For smaller values of the heavy Higgs-boson mass between 200 to 400 GeV the electroweak corrections of the BPs are of moderate size and are of the order of a few percent. They coincide with what one expects from figure 10 in this mass range. Approaching heavy Higgs-boson masses of 500 to 600 GeV the electroweak corrections of the BPs are large and positive in accordance with figure 10. All BPs which only differ in the sign of $\sin\alpha$ are very close to each other, except for the benchmark point BHM600±. The latter BP is close to the location where in figure 10 the percentage corrections become large, changing sign from positive to negative, and the curve has a steep slope. Thus the percentage correction vastly changes in a small window of a few GeV explaining the different percentage correction for BHM600− and BHM600+. The large negative size of the electroweak corrections for the benchmark points BHM700 and BHM800 has the same reason as the large negative corrections as discussed in the analysis of figure 10, i.e. the squared modulus of the LO amplitude becomes small.

Now we compare again the results for the electroweak percentage corrections in the three different renormalization schemes for the mixing angle α under consideration in this paper for the two decay processes $H_{\rm l} \to \gamma + \gamma$ and $H_{\rm h} \to \gamma + \gamma$. The reasoning for the choices of $\sin\alpha$ and $\tan\beta$ in figure 12 and also in figure 13 is the same as the one described already in section 4.1 for figures 9 and 10.

JHEP11(2023)113

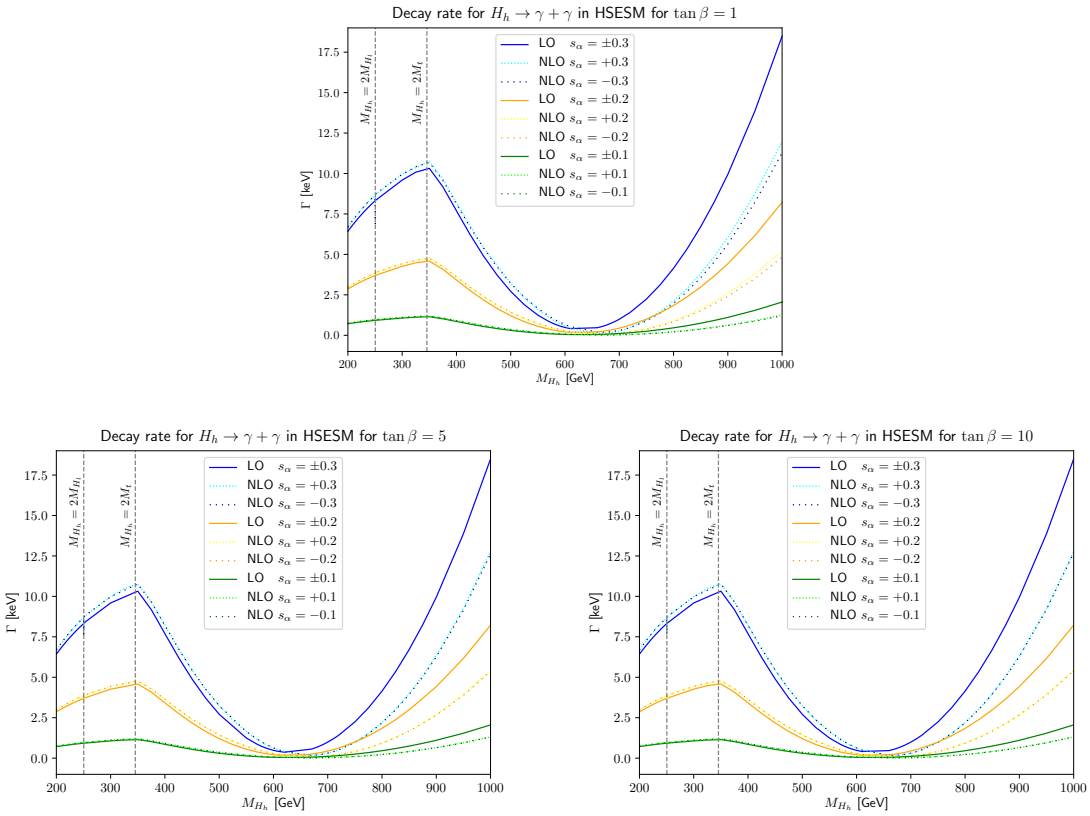

Figure 11. Behaviour of the LO and NLO partial decay width for $H_h \to \gamma + \gamma$ for $\tan\beta = 1, 5, 10$ with varying values of $\sin\alpha$. The vertical dashed lines indicate the location of the $H_l H_l$- and tt-thresholds.

BP	$\delta_{\rm EW}$
BHM200−	4.0
BHM200+	4.0
BHM300−	3.8
BHM300+	3.9
BHM400a−	6.0
BHM400a+	6.7

BP	$\delta_{\rm EW}$
BHM400b	6.7
BHM500a−	19.2
BHM500a+	19.1
BHM500b	19.1
BHM600−	35.1
BHM600+	29.6

BP	$\delta_{\rm EW}$
BHM700a−	−70.3
BHM700a+	−71.0
BHM700b	−71.0
BHM800a−	−50.0
BHM800a+	−49.4
BHM800b	−49.4

Table 5. The electroweak percentage corrections $\delta_{\rm EW}$ [%] for the decay process $H_{\rm h} \to \gamma + \gamma$ are shown for a renormalization of the mixing angle α in the OS scheme.

JHEP11(2023)113

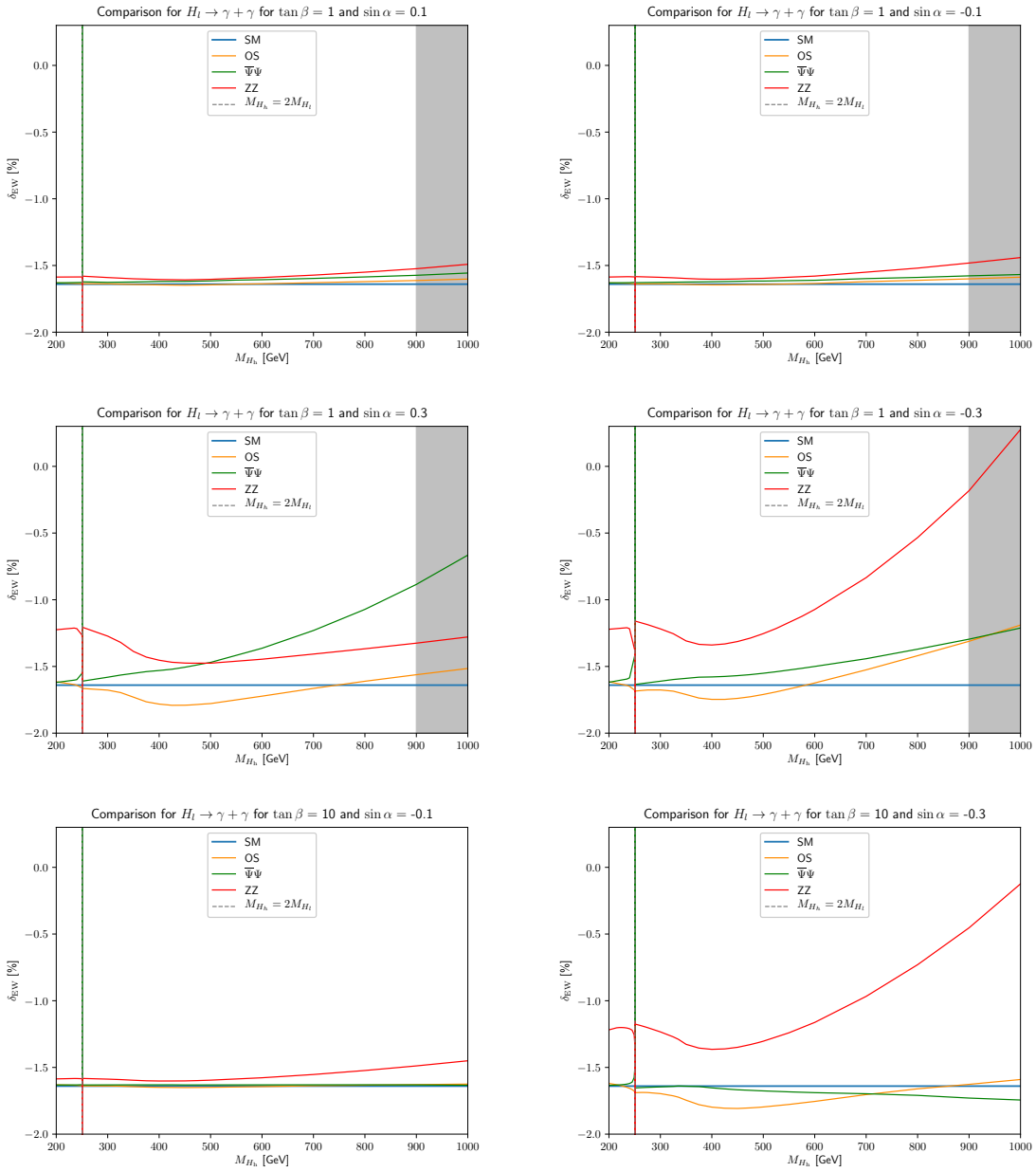

Figure 12. Comparison of the different renormalization schemes for the mixing angle α for the decay process $H_l \to \gamma + \gamma$ in the HSESM for $\tan\beta = 1, 10$ with varying values of $\sin\alpha$. The SM limit is shown by the blue line.

JHEP11(2023)113

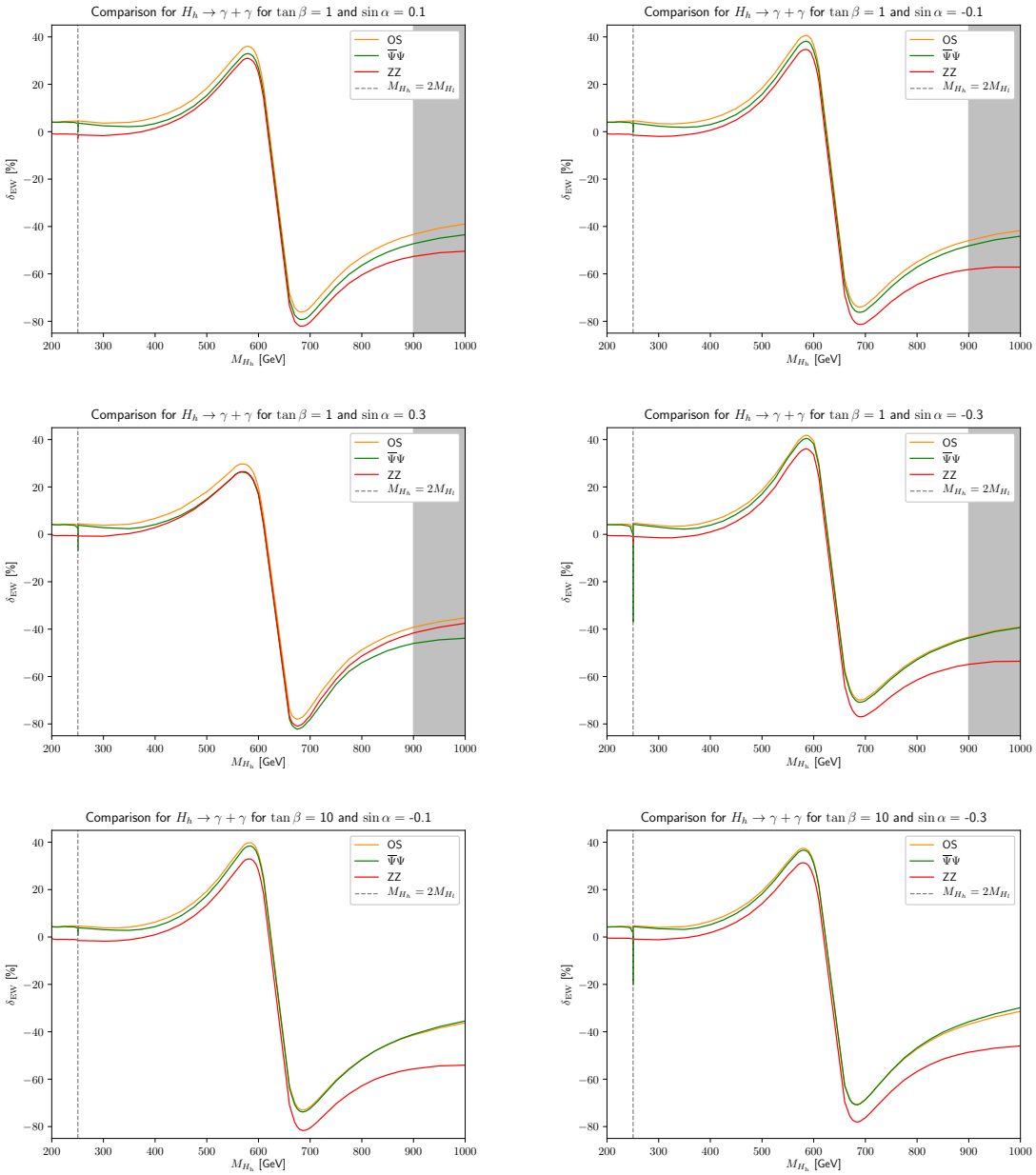

Figure 13. Comparison of the different renormalization schemes for the mixing angle α for the decay $H_h \to \gamma + \gamma$ in the HSESM for $\tan\beta = 1, 10$ with varying values of $\sin\alpha$.

JHEP11(2023)113

We start in figure 12 with the NLO electroweak percentage corrections as a function of the heavy Higgs-boson mass M_{H_h} for the process $H_l \to \gamma + \gamma$. All six plots show again the same range for the electroweak percentage corrections and the heavy Higgs-boson mass in order to allow for an easy comparison of the different scenarios. The comparison plots show features similar to the case of $g + g \to H_l$. As before, the two process dependent ZZ- and $\overline{\Psi}\Psi$-schemes contain the artificially introduced threshold singularities for $M_{H_h} = 2M_{H_l}$. For the values $\sin\alpha = \pm 0.1$ the three schemes are hardly distinguishable since we are close to the SM case. However, also for this process the ZZ scheme is shifted upwards from the SM for all values of $\tan\beta$ and $\sin\alpha$. Its sensitivity to the sign of $\sin\alpha$ is demonstrated by comparing the plots with $\tan\beta = 1$ and $\sin\alpha = \pm 0.3$. In particular, for $\sin\alpha = -0.3$ we observe again a strong dependence of the ZZ scheme on M_{H_h}. In addition, the $\overline{\Psi}\Psi$ scheme shows the strongest dependence on $\tan\beta$. Despite the fact that the differences for $\sin\alpha = -0.3$ look large we want to note that the percentage corrections only cover a small range of about 1.5%, so that also the differences between the schemes are at most of the same size.

In figure 13 we compare likewise the three different renormalization schemes for the NLO electroweak percentage corrections of the decay $H_h \to \gamma + \gamma$. All three schemes show the threshold singularity at $M_{H_h} = 2M_{H_l}$, with a strong dependence of the size of the cusp on the scheme. As it was the case for heavy Higgs-boson production in gluon fusion the lowest value of the electroweak percentage corrections at this threshold is obtained in the $\overline{\Psi}\Psi$ scheme, whereas barely any cusp is visible in the ZZ scheme. Another similarity to the process $g + g \to H_h$ is the fact that the ZZ scheme is shifted downwards compared to the OS scheme. In contrast to all other processes, the ZZ scheme here does not show the strongest M_{H_h} dependence for negative values of $\sin\alpha$ and large heavy Higgs-boson mass M_{H_h}. Indeed in this mass region the dependence on M_{H_h} is milder in this case than for positive $\sin\alpha$. For $\sin\alpha = -0.3$ large differences between the ZZ scheme and the other two schemes exist and the ZZ scheme shows a weak dependence on the heavy Higgs-boson mass M_{H_h}. The $\overline{\Psi}\Psi$ scheme again shows the strongest dependence on $\tan\beta$ for $\sin\alpha = +0.3$ when going from $\tan\beta = 1$ to $\tan\beta = 10$. Since for large $\tan\beta$ the corrections are insensitive to the sign of $\sin\alpha$, the corrections for $\tan\beta = 10$ and $\sin\alpha = +0.3$ are comparable to the corrections for $\tan\beta = 10$ and $\sin\alpha = -0.3$.

The numerical comparison of the results in the different renormalization schemes justifies our choice of the OS scheme as reference scheme. In fact the $\overline{\Psi}\Psi$ and ZZ schemes show artificial features connected to the processes which underly the renormalization as for instance the threshold singularities at $M_{H_h} = 2M_{H_l}$ for the light Higgs-boson production and decay or the large corrections in the ZZ scheme in some regions of the parametric space.

5 Summary and conclusion

We have computed the two-loop electroweak corrections for four loop-induced processes in the real Higgs-Singlet Extensions of the Standard Model (HSESM). For the Higgs-boson production we considered the light and heavy Higgs-boson production in gluon fusion. For

JHEP11(2023)113

the Higgs-boson decay we considered the light and heavy Higgs-boson decays into two photons. The HSESM has three additional new input parameters compared to the Standard Model (SM) which are the new heavy Higgs-boson mass, the mixing angle α and the ratio of the two vacuum expectation values $\tan\beta$. The latter needs not to be renormalized for the above processes, while for the mixing angle α we consider three renormalization schemes from literature among which we choose the on-shell scheme for our final results.

The few new parameters of the HSESM allow us to provide the electroweak percentage corrections to these processes for scans over a wide range of the new input parameters. In addition we also provide the results for benchmark scenarios which have been collected by the Higgs cross section working group.

For the considered range of the new input parameters ($|\sin\alpha| \leq 0.3$, $1 \leq \tan\beta \leq 10$, $M_{H_h} \leq 1\,\text{TeV}$) the electroweak corrections for light Higgs-boson production through gluon fusion and for the decay into two photons are in both cases very close to the SM. In the same range the electroweak corrections for heavy Higgs-boson production are negative and can reach up to about -10% in the on-shell scheme for large heavy Higgs-boson masses. The heavy Higgs-boson decay into two photons shows an interesting feature. The electroweak percentage corrections change here from large positive corrections to large negative corrections within about $\pm 50\,\text{GeV}$ for heavy Higgs-boson masses of around 630 GeV. This feature is inherited from the leading-order amplitude which becomes very small in this region explaining thus the large size of the electroweak corrections.

Acknowledgments

We would like to thank Ansgar Denner, Stefan Dittmaier, Jean-Nicolas Lang and Giampiero Passarino for valuable discussions. The work of B.S. and C.S. was supported by the Deutsche Forschungsgemeinschaft (DFG) under contract STU 615/2-1, project number 436076086.

References

[1] ATLAS collaboration, *Observation of a new particle in the search for the Standard Model Higgs boson with the ATLAS detector at the LHC*, *Phys. Lett. B* **716** (2012) 1 [arXiv:1207.7214] [INSPIRE].

[2] CMS collaboration, *Observation of a New Boson at a Mass of* 125 *GeV with the CMS Experiment at the LHC*, *Phys. Lett. B* **716** (2012) 30 [arXiv:1207.7235] [INSPIRE].

[3] V. Silveira and A. Zee, *Scalar phantoms*, *Phys. Lett. B* **161** (1985) 136 [INSPIRE].

[4] J. McDonald, *Gauge singlet scalars as cold dark matter*, *Phys. Rev. D* **50** (1994) 3637 [hep-ph/0702143] [INSPIRE].

[5] T. Binoth and J.J. van der Bij, *Influence of strongly coupled, hidden scalars on Higgs signals*, *Z. Phys. C* **75** (1997) 17 [hep-ph/9608245] [INSPIRE].

JHEP11(2023)113

[6] R.M. Schabinger and J.D. Wells, *A Minimal spontaneously broken hidden sector and its impact on Higgs boson physics at the large hadron collider*, *Phys. Rev. D* **72** (2005) 093007 [hep-ph/0509209] [INSPIRE].

[7] B. Patt and F. Wilczek, *Higgs-field portal into hidden sectors*, hep-ph/0605188 [INSPIRE].

[8] M. Bowen, Y. Cui and J.D. Wells, *Narrow trans-TeV Higgs bosons and $H \to hh$ decays: Two LHC search paths for a hidden sector Higgs boson*, *JHEP* **03** (2007) 036 [hep-ph/0701035] [INSPIRE].

[9] V. Barger et al., *LHC Phenomenology of an Extended Standard Model with a Real Scalar Singlet*, *Phys. Rev. D* **77** (2008) 035005 [arXiv:0706.4311] [INSPIRE].

[10] T. Robens and T. Stefaniak, *Status of the Higgs Singlet Extension of the Standard Model after LHC Run 1*, *Eur. Phys. J. C* **75** (2015) 104 [arXiv:1501.02234] [INSPIRE].

[11] T. Robens, *Constraining Extended Scalar Sectors at Current and Future Colliders — An Update*, *Springer Proc. Phys.* **292** (2023) 141 [arXiv:2209.15544] [INSPIRE].

[12] Particle Data Group collaboration, *Review of Particle Physics*, *PTEP* **2020** (2020) 083C01 [INSPIRE].

[13] V. Barger et al., *Complex Singlet Extension of the Standard Model*, *Phys. Rev. D* **79** (2009) 015018 [arXiv:0811.0393] [INSPIRE].

[14] ATLAS collaboration, *Constraints on new phenomena via Higgs boson couplings and invisible decays with the ATLAS detector*, *JHEP* **11** (2015) 206 [arXiv:1509.00672] [INSPIRE].

[15] CMS collaboration, *Search for a Higgs boson in the mass range from 145 to 1000 GeV decaying to a pair of W or Z bosons*, *JHEP* **10** (2015) 144 [arXiv:1504.00936] [INSPIRE].

[16] CMS collaboration, *Search for a new scalar resonance decaying to a pair of Z bosons in proton-proton collisions at $\sqrt{s} = 13$ TeV*, *JHEP* **06** (2018) 127 [*Erratum ibid.* **03** (2019) 128] [arXiv:1804.01939] [INSPIRE].

[17] ATLAS collaboration, *Combination of searches for heavy resonances decaying into bosonic and leptonic final states using 36 fb^{-1} of proton-proton collision data at $\sqrt{s} = 13$ TeV with the ATLAS detector*, *Phys. Rev. D* **98** (2018) 052008 [arXiv:1808.02380] [INSPIRE].

[18] ATLAS collaboration, *Search for heavy resonances decaying into a pair of Z bosons in the $\ell^+\ell^-\ell'^+\ell'^-$ and $\ell^+\ell^-\nu\bar{\nu}$ final states using 139 fb^{-1} of proton-proton collisions at $\sqrt{s} = 13$ TeV with the ATLAS detector*, *Eur. Phys. J. C* **81** (2021) 332 [arXiv:2009.14791] [INSPIRE].

[19] ATLAS collaboration, *Search for Higgs boson pair production in the two bottom quarks plus two photons final state in pp collisions at $\sqrt{s} = 13$ TeV with the ATLAS detector*, *Phys. Rev. D* **106** (2022) 052001 [arXiv:2112.11876] [INSPIRE].

[20] ATLAS collaboration, *Search for resonant pair production of Higgs bosons in the $b\bar{b}b\bar{b}$ final state using pp collisions at $\sqrt{s} = 13$ TeV with the ATLAS detector*, *Phys. Rev. D* **105** (2022) 092002 [arXiv:2202.07288] [INSPIRE].

[21] ATLAS collaboration, *Combination of searches for Higgs boson pairs in pp collisions at $\sqrt{s} = 13$ TeV with the ATLAS detector*, *Phys. Lett. B* **800** (2020) 135103 [arXiv:1906.02025] [INSPIRE].

[22] A. Denner, J.-N. Lang and S. Uccirati, *NLO electroweak corrections in extended Higgs Sectors with RECOLA2*, *JHEP* **07** (2017) 087 [arXiv:1705.06053] [INSPIRE].

JHEP11(2023)113

[23] L. Altenkamp, M. Boggia and S. Dittmaier, *Precision calculations for $h \to WW/ZZ \to 4$ fermions in a Singlet Extension of the Standard Model with Prophecy4f*, *JHEP* **04** (2018) 062 [arXiv:1801.07291] [INSPIRE].

[24] A. Denner, S. Dittmaier and J.-N. Lang, *Renormalization of mixing angles*, *JHEP* **11** (2018) 104 [arXiv:1808.03466] [INSPIRE].

[25] N. Kauer, A. Lind, P. Maierhöfer and W. Song, *Higgs interference effects at the one-loop level in the 1-Higgs-Singlet extension of the Standard Model*, *JHEP* **07** (2019) 108 [arXiv:1905.03296] [INSPIRE].

[26] P. Basler, S. Dawson, C. Englert and M. Mühlleitner, *Di-Higgs boson peaks and top valleys: Interference effects in Higgs sector extensions*, *Phys. Rev. D* **101** (2020) 015019 [arXiv:1909.09987] [INSPIRE].

[27] F. Bojarski, G. Chalons, D. Lopez-Val and T. Robens, *Heavy to light Higgs boson decays at NLO in the Singlet Extension of the Standard Model*, *JHEP* **02** (2016) 147 [arXiv:1511.08120] [INSPIRE].

[28] M. Boggia, R. Gomez-Ambrosio and G. Passarino, *Low energy behaviour of standard model extensions*, *JHEP* **05** (2016) 162 [arXiv:1603.03660] [INSPIRE].

[29] M. Jiang, N. Craig, Y.-Y. Li and D. Sutherland, *Complete one-loop matching for a singlet scalar in the Standard Model EFT*, *JHEP* **02** (2019) 031 [*Erratum ibid.* **01** (2021) 135] [arXiv:1811.08878] [INSPIRE].

[30] U. Haisch et al., *Singlet night in Feynman-ville: one-loop matching of a real scalar*, *JHEP* **04** (2020) 164 [*Erratum ibid.* **07** (2020) 066] [arXiv:2003.05936] [INSPIRE].

[31] S. Dittmaier, S. Schuhmacher and M. Stahlhofen, *Integrating out heavy fields in the path integral using the background-field method: general formalism*, *Eur. Phys. J. C* **81** (2021) 826 [arXiv:2102.12020] [INSPIRE].

[32] J. Ellis, K. Mimasu and F. Zampedri, *Dimension-8 SMEFT analysis of minimal scalar field extensions of the Standard Model*, *JHEP* **10** (2023) 051 [arXiv:2304.06663] [INSPIRE].

[33] T. Robens, *Extended scalar sectors at current and future colliders*, in the proceedings of the *55th Rencontres de Moriond on QCD and High Energy Interactions*, Online Italy, MArch 27–April 03 (2021) [arXiv:2105.07719] [INSPIRE].

[34] A. Ilnicka, T. Robens and T. Stefaniak, *Constraining Extended Scalar Sectors at the LHC and beyond*, *Mod. Phys. Lett. A* **33** (2018) 1830007 [arXiv:1803.03594] [INSPIRE].

[35] R. Costa, M. Mühlleitner, M.O.P. Sampaio and R. Santos, *Singlet Extensions of the Standard Model at LHC Run 2: Benchmarks and Comparison with the NMSSM*, *JHEP* **06** (2016) 034 [arXiv:1512.05355] [INSPIRE].

[36] G.M. Pruna and T. Robens, *Higgs singlet extension parameter space in the light of the LHC discovery*, *Phys. Rev. D* **88** (2013) 115012 [arXiv:1303.1150] [INSPIRE].

[37] T. Robens and T. Stefaniak, *LHC Benchmark Scenarios for the Real Higgs Singlet Extension of the Standard Model*, *Eur. Phys. J. C* **76** (2016) 268 [arXiv:1601.07880] [INSPIRE].

[38] LHC Higgs Cross Section Working Group collaboration, *Handbook of LHC Higgs Cross Sections: 4. Deciphering the Nature of the Higgs Sector*, arXiv:1610.07922 [DOI:10.23731/CYRM-2017-002] [INSPIRE].

JHEP11(2023)113

[39] U. Aglietti, R. Bonciani, G. Degrassi and A. Vicini, *Two loop light fermion contribution to Higgs production and decays*, *Phys. Lett. B* **595** (2004) 432 [hep-ph/0404071] [INSPIRE].

[40] G. Degrassi and F. Maltoni, *Two-loop electroweak corrections to Higgs production at hadron colliders*, *Phys. Lett. B* **600** (2004) 255 [hep-ph/0407249] [INSPIRE].

[41] G. Passarino, C. Sturm and S. Uccirati, *Complete Two-Loop Corrections to $H \to \gamma\gamma$*, *Phys. Lett. B* **655** (2007) 298 [arXiv:0707.1401] [INSPIRE].

[42] S. Actis, G. Passarino, C. Sturm and S. Uccirati, *NLO Electroweak Corrections to Higgs Boson Production at Hadron Colliders*, *Phys. Lett. B* **670** (2008) 12 [arXiv:0809.1301] [INSPIRE].

[43] S. Actis, G. Passarino, C. Sturm and S. Uccirati, *NNLO Computational Techniques: The Cases $H \to \gamma\gamma$ and $H \to gg$*, *Nucl. Phys. B* **811** (2009) 182 [arXiv:0809.3667] [INSPIRE].

[44] C. Anastasiou et al., *High precision determination of the gluon fusion Higgs boson cross-section at the LHC*, *JHEP* **05** (2016) 058 [arXiv:1602.00695] [INSPIRE].

[45] C. Anastasiou et al., *Higgs Boson Gluon-Fusion Production in QCD at Three Loops*, *Phys. Rev. Lett.* **114** (2015) 212001 [arXiv:1503.06056] [INSPIRE].

[46] C. Sturm, *Higher order QCD results for the fermionic contributions of the Higgs-boson decay into two photons and the decoupling function for the $\overline{MS}$ renormalized fine-structure constant*, *Eur. Phys. J. C* **74** (2014) 2978 [arXiv:1404.3433] [INSPIRE].

[47] J. Davies and F. Herren, *Higgs boson decay into photons at four loops*, *Phys. Rev. D* **104** (2021) 053010 [arXiv:2104.12780] [INSPIRE].

[48] M. Bonetti, K. Melnikov and L. Tancredi, *Higher order corrections to mixed QCD-EW contributions to Higgs boson production in gluon fusion*, *Phys. Rev. D* **97** (2018) 056017 [*Erratum ibid.* **97** (2018) 099906] [arXiv:1801.10403] [INSPIRE].

[49] G. Passarino, C. Sturm and S. Uccirati, *Complete Electroweak Corrections to Higgs production in a Standard Model with four generations at the LHC*, *Phys. Lett. B* **706** (2011) 195 [arXiv:1108.2025] [INSPIRE].

[50] A. Denner et al., *Higgs Production and Decay with a Fourth Standard-Model-Like Fermion Generation*, *Eur. Phys. J. C* **72** (2012) 1992 [arXiv:1111.6395] [INSPIRE].

[51] A. Denner, L. Jenniches, J.-N. Lang and C. Sturm, *Gauge-independent $\overline{MS}$ renormalization in the 2HDM*, *JHEP* **09** (2016) 115 [arXiv:1607.07352] [INSPIRE].

[52] L. Jenniches, C. Sturm and S. Uccirati, *Electroweak corrections in the 2HDM for neutral scalar Higgs-boson production through gluon fusion*, *JHEP* **09** (2018) 017 [arXiv:1805.05869] [INSPIRE].

[53] L. Jenniches, C. Sturm and S. Uccirati, *Higgs-boson production through gluon fusion in the 2HDM with electroweak corrections*, *PoS* **RADCOR2017** (2018) 065 [INSPIRE].

[54] J.R. Ellis, M.K. Gaillard and D.V. Nanopoulos, *A Phenomenological Profile of the Higgs Boson*, *Nucl. Phys. B* **106** (1976) 292 [INSPIRE].

[55] M.A. Shifman, A.I. Vainshtein, M.B. Voloshin and V.I. Zakharov, *Low-Energy Theorems for Higgs Boson Couplings to Photons*, *Sov. J. Nucl. Phys.* **30** (1979) 711 [INSPIRE].

[56] K.G. Chetyrkin, J.H. Kühn and M. Steinhauser, *RunDec: A Mathematica package for running and decoupling of the strong coupling and quark masses*, *Comput. Phys. Commun.* **133** (2000) 43 [hep-ph/0004189] [INSPIRE].

JHEP11(2023)113

[57] A. Alloul et al., *FeynRules 2.0 — A complete toolbox for tree-level phenomenology*, *Comput. Phys. Commun.* **185** (2014) 2250 [arXiv:1310.1921] [INSPIRE].

[58] N.D. Christensen and C. Duhr, *FeynRules — Feynman rules made easy*, *Comput. Phys. Commun.* **180** (2009) 1614 [arXiv:0806.4194] [INSPIRE].

[59] P. Nogueira, *Automatic Feynman graph generation*, *J. Comput. Phys.* **105** (1993) 279 [INSPIRE].

[60] J.A.M. Vermaseren, *New features of FORM*, math-ph/0010025 [INSPIRE].

[61] B. Ruijl, T. Ueda and J. Vermaseren, *FORM version 4.2*, arXiv:1707.06453 [INSPIRE].

[62] G. Passarino and S. Uccirati, *Algebraic numerical evaluation of Feynman diagrams: Two loop selfenergies*, *Nucl. Phys. B* **629** (2002) 97 [hep-ph/0112004] [INSPIRE].

[63] A. Ferroglia, M. Passera, G. Passarino and S. Uccirati, *Two loop vertices in quantum field theory: Infrared convergent scalar configurations*, *Nucl. Phys. B* **680** (2004) 199 [hep-ph/0311186] [INSPIRE].

[64] G. Passarino and S. Uccirati, *Two-loop vertices in quantum field theory: Infrared and collinear divergent configurations*, *Nucl. Phys. B* **747** (2006) 113 [hep-ph/0603121] [INSPIRE].

[65] N.M. Korobov, *The approximate calculation of multiple integrals using number theoretic methods*, *Dokl. Acad. Nauk SSSR* **115** (1957) 1062.

[66] N.M. Korobov, *Number-theoretic methods in approximate analysis*, Fizmatgiz, Moscow (1963).

[67] H. Conroy, *Molecular Schrödinger Equation. VIII. A New Method for the Evaluation of Multidimensional Integrals* *J. Chem. Phys.* **47** (1967) 5307.

[68] A. Denner, S. Dittmaier, M. Roth and D. Wackeroth, *Predictions for all processes $e^+e^- \to 4$ fermions + γ*, *Nucl. Phys. B* **560** (1999) 33 [hep-ph/9904472] [INSPIRE].

[69] A. Denner, S. Dittmaier, M. Roth and L.H. Wieders, *Electroweak corrections to charged-current $e + e- \to 4$ fermion processes: Technical details and further results*, *Nucl. Phys. B* **724** (2005) 247 [hep-ph/0505042] [INSPIRE].

[70] A. Denner and S. Dittmaier, *The Complex-mass scheme for perturbative calculations with unstable particles*, *Nucl. Phys. B Proc. Suppl.* **160** (2006) 22 [hep-ph/0605312] [INSPIRE].

[71] J. Fleischer and F. Jegerlehner, *Radiative Corrections to Higgs Decays in the Extended Weinberg-Salam Model*, *Phys. Rev. D* **23** (1981) 2001 [INSPIRE].

[72] S. Actis, A. Ferroglia, M. Passera and G. Passarino, *Two-Loop Renormalization in the Standard Model. Part I: Prolegomena*, *Nucl. Phys. B* **777** (2007) 1 [hep-ph/0612122] [INSPIRE].

[73] S. Dittmaier and H. Rzehak, *Electroweak renormalization based on gauge-invariant vacuum expectation values of non-linear Higgs representations. Part I. Standard Model*, *JHEP* **05** (2022) 125 [arXiv:2203.07236] [INSPIRE].

[74] S. Dittmaier and H. Rzehak, *Electroweak renormalization based on gauge-invariant vacuum expectation values of non-linear Higgs representations. Part II. Extended Higgs sectors*, *JHEP* **08** (2022) 245 [arXiv:2206.01479] [INSPIRE].

[75] S. Kanemura, Y. Okada, E. Senaha and C.-P. Yuan, *Higgs coupling constants as a probe of new physics*, *Phys. Rev. D* **70** (2004) 115002 [hep-ph/0408364] [INSPIRE].

JHEP11(2023)113

[76] A. Denner, J.-N. Lang and S. Uccirati, *Recola2: REcursive Computation of One-Loop Amplitudes 2*, *Comput. Phys. Commun.* **224** (2018) 346 [arXiv:1711.07388] [INSPIRE].

[77] A. Freitas and D. Stöckinger, *Gauge dependence and renormalization of* $\tan\beta$ *in the MSSM*, *Phys. Rev. D* **66** (2002) 095014 [hep-ph/0205281] [INSPIRE].

[78] B. Summ, C. Sturm and S. Uccirati, *Electroweak corrections to* $gg \to H$ *and* $H \to \gamma\gamma$ *in the singlet extended Standard Model*, DOI:10.5281/ZENODO.7254998.

[79] S. Actis, G. Passarino, C. Sturm and S. Uccirati, *Two-Loop Threshold Singularities, Unstable Particles and Complex Masses*, *Phys. Lett. B* **669** (2008) 62 [arXiv:0809.1302] [INSPIRE].

JHEP11(2023)113